MINISTRY OF EDUCATION AND RESEARCH





THE ANNALS OF "DUNAREA DE JOS" UNIVERSITY OF GALATI

Fascicle IX METALLURGY AND MATERIALS SCIENCE

YEAR XLIII (XLVIII) September 2025, no. 3

ISSN 2668-4748; e-ISSN 2668-4756



EDITORIAL BOARD

EDITOR-IN-CHIEF

Assist. Prof. Marius BODOR - "Dunarea de Jos" University of Galati, Romania

SCIENTIFIC ADVISORY COMMITTEE

Assist. Prof. Dragos-Cristian ACHITEI - "Gheorghe Asachi" Technical University Iasi, Romania

Assoc. Prof. Stefan BALTA - "Dunarea de Jos" University of Galati, Romania

Prof. Sorin-Ștefan BIRIS - Politehnica University of Bucuresti, Romania

Assist. Prof. Chenna Rao BORRA - Indian Institute of Technology, Republic of India

Prof. Acad. Ion BOSTAN - Technical University of Moldova, the Republic of Moldova

Researcher Mihai BOTAN - The National Institute of Aerospace Research, Romania

Prof. Vasile BRATU - Valahia University of Targoviste, Romania

Prof. Francisco Manuel BRAZ FERNANDES - New University of Lisbon Caparica, Portugal

Prof. Bart Van der BRUGGEN - Katholieke Universiteit Leuven, Belgium

Prof. Acad. Valeriu CANTSER - Academy of the Republic of Moldova

Prof. Valeriu DULGHERU - Technical University of Moldova, the Republic of Moldova

Prof. Gheorghe GURAU - "Dunarea de Jos" University of Galati, Romania

Assist. Prof. Gina Genoveva ISTRATE - "Dunarea de Jos" University of Galati, Romania

Assist. Prof. Nora JULLOK - Universiti Malaysia Perlis, Malaysia

Prof. Rodrigo MARTINS - NOVA University of Lisbon, Portugal

Prof. Valer MICLE - Technical University of Cluj Napoca, Romania

Prof. Strul MOISA – Ben Gurion University of the Negev, Israel

Assist. Prof. Priyanka MONDAL - CSIR-Central Glass and Ceramic Research Institute, India

Prof. Daniel MUNTEANU - "Transilvania" University of Brasov, Romania

Assoc. Prof. Alina MURESAN - "Dunarea de Jos" University of Galati, Romania

Assist. Prof. Manuela-Cristina PERJU - "Gheorghe Asachi" Technical University Iasi, Romania

Prof. Cristian PREDESCU - Politehnica University of Bucuresti, Romania

Prof. Iulian RIPOSAN - Politehnica University of Bucuresti, Romania

Prof. Antonio de SAJA - University of Valladolid, Spain

Assist. Prof. Rafael M. SANTOS – University of Guelph, Canada

Prof. Ion SANDU - "Al. I. Cuza" University of Iasi, Romania

Prof. Mircea Horia TIEREAN - "Transilvania" University of Brasov, Romania

Prof. Ioan VIDA-SIMITI - Technical University of Cluj Napoca, Romania

Assoc. Prof. Petrica VIZUREANU - "Gheorghe Asachi" Technical University Iasi, Romania

EDITING SECRETARY

Assist. Prof. Marius BODOR - "Dunarea de Jos" University of Galati, Romania

Assist. Nicoleta BOGATU - "Dunarea de Jos" University of Galati, Romania

Assist. Prof. Eliza DANAILA - "Dunarea de Jos" University of Galati, Romania

Assist. Prof. Florin Bogdan MARIN - "Dunarea de Jos" University of Galati, Romania

Assist. Prof. Mihaela MARIN - "Dunarea de Jos" University of Galati, Romania



N°. 3 - 2025, ISSN 2668-4748; e-ISSN 2668-4756 Volume DOI: https://doi.org/10.35219/mms.2025.3

Table of Contents

1. Mihaela MARIN, Roxana OPREA, Florin-Bogdan MARIN - A Comparative Evaluation of Technical, Financial, and Imaging Performance Between 1.5 Tesla and 3 Tesla MRI Systems for Clinical Applications	5
2. Beatrice Daniela TUDOR - Research on Creating Decorative Objects from Glass Waste Through Thermoforming	10
3. Beatrice Daniela TUDOR - Studies and Research on Obtaining Glass Inlays in Metal	17
4. Ştefănică FRANGU, Ioan ŞUŞNEA - How Blockchain Can Reshape the Supply Chain of Steel for an Industrial Complex	23
5. Florin-Bogdan MARIN, Gheorghe GURĂU, Florin TURCU, Mihaela MARIN - Numerical Simulation and Optimization of Aluminum Die Casting for Enhanced Part Quality	28
6. Florin-Bogdan MARIN, Gheorghe GURĂU, Lucian GRIGORAŞ, Mihaela MARIN - Simulation-Based Design of Parametric Origami Structures for Blast and Ballistic Protection	35
7. Florin-Bogdan MARIN, Cristina-Daniela STAICU (MĂRIAN), Mihaela MARIN - Development and Testing of a Seismic-Responsive IoT-Based Safety System for Gas Distribution Networks	42



N°. 3 - 2025, ISSN 2668-4748; e-ISSN 2668-4756 Volume DOI: <u>https://doi.org/10.35219/mms.2025.3</u>



N°. 3 - 2025, ISSN 2668-4748; e-ISSN 2668-4756 Article DOI: https://doi.org/10.35219/mms.2025.3.01

A COMPARATIVE EVALUATION OF TECHNICAL, FINANCIAL, AND IMAGING PERFORMANCE BETWEEN 1.5 TESLA AND 3 TESLA MRI SYSTEMS FOR CLINICAL APPLICATIONS

Mihaela MARIN^{1,2}, Roxana OPREA¹, Florin-Bogdan MARIN^{1,2}

¹ "Dunarea de Jos" University of Galati, Romania

² Interdisciplinary Research Centre in the Field of Eco-Nano Technology and Advance Materials CC-ITI, Faculty of Engineering, "Dunarea de Jos" University of Galati, Romania, 47 Domnească Street, RO-800008, Galați, Romania

e-mail: mihaela.marin@ugal.ro

ABSTRACT

This paper presents a structured comparative assessment between 1.5 T and 3 T Magnetic Resonance Imaging (MRI) systems, focusing on technical specifications, economic impact, and diagnostic image quality. Data compiled from manufacturer documentation and clinical usage evaluations reveal that 3 T systems provide higher spatial resolution, improved signal-to-noise ratio (SNR), shorter image acquisition times, and reduced artefact levels. However, these advantages come with substantially increased acquisition and operational costs. The study concludes with recommendations tailored to clinical needs, highlighting that 3 T systems are suited for advanced imaging applications, while 1.5 T platforms remain economically viable for standard diagnostic procedures.

KEYWORDS: magnetic resonance imaging, 1.5 Tesla MRI, 3 Tesla MRI, diagnostic imaging, technical performance

1. Introduction

Magnetic Resonance Imaging (MRI) plays a pivotal role in modern diagnostic radiology due to its ability to produce detailed soft tissue images without ionizing radiation. The selection of magnetic field strength significantly influences image quality, workflow efficiency, and diagnostic precision. In clinical practice, both 1.5 T and 3 T MRI systems are prevalent, representing distinct trade-offs between performance and cost.

Several recent comparative studies have confirmed that 3 T scanners deliver markedly higher signal-to-noise ratio (SNR) and superior spatial resolution compared to 1.5 T systems [1]. One analysis of knee MRI demonstrated that 3 T systems allowed a substantial reduction in scan time while preserving diagnostic quality [2]. Comparative evaluations in brain imaging revealed that 3 T MRI systems offered better lesion conspicuity and contrast-to-noise ratio than 1.5 T platforms [3]. Higher SNR at 3 T enables finer anatomical detail, allowing for improved detection of small structural abnormalities [4]. Moreover, 3 T systems reduce the incidence of motion artifacts through faster

acquisitions, which enhances image fidelity during patient exams [5].

However, recent clinical reports have highlighted that 3 T systems may be more prone to susceptibility and dielectric artifacts, particularly in abdominal and spinal applications [6]. Advances in MRI technology, including optimized pulse sequences and coil design, have mitigated these limitations, making 1.5 T imaging more competitive [7]. A modern prospective study comparing 1.5 T and 3 T in neurosurgical planning found equivalent diagnostic performance when optimized protocols were applied on both systems [8].

Beyond image quality parameters, it is essential to evaluate the economic impact of MRI system selection. A study of intraoperative high field 3 T MRI demonstrated significant incremental cost but also identified operational advantages that enhanced surgical outcomes [9]. Another cost-benefit analysis reported that, despite higher initial investment and maintenance expenses, 3 T implementation can be justified in high volume or specialist centres [10].

Recent technological innovations, such as AI-based noise reduction and compressed sensing, have further expanded the clinical utility of both 1.5 T and



N°. 3 - 2025, ISSN 2668-4748; e-ISSN 2668-4756

Article DOI: https://doi.org/10.35219/mms.2025.3.01

3 T systems, enhancing image quality and reducing scan time [11]. Studies on AI-aided diagnosis have shown that 3 T MRI combined with machine learning models has improved detection rates neurodegenerative conditions [12]. Similarly, the use of ultra-high resolution cartilage imaging protocols at 3 T has yielded superior morphological detail compared to 1.5 T systems [13]. Research on patient comfort highlighted that shorter scan durations at 3 T reduce motion related rescans and improve throughput [14]. In contrast, low field 1.5 T MRI benefits from increased availability of compatible implants and lower susceptibility artifacts around metallic prosthetics [15]. Finally, economic models suggest that a hybrid MRI fleet combining 1.5 T and 3 T systems may deliver optimal value across diverse clinical workloads [16].

In summary, the decision between 1.5 T and 3 T MRI deployment should be driven by clinical requirements, technical constraints, and institutional budget considerations This study integrates these aspects by examining technical performance, image quality, and lifecycle costs to support evidence-based decision making in MRI acquisition.

2. Experimental procedure

This study involved a structured analysis of technical documentation, operational parameters, and economic reports for 1.5 Tesla and 3 Tesla Magnetic Resonance Imaging (MRI) systems. The investigation focused on evaluating performance indicators that directly influence diagnostic quality and clinical workflow. Data were collected from verified manufacturer specifications, peer-reviewed technical sheets, and practical implementation reports in hospital settings.

For technical performance evaluation, five core parameters were selected: magnetic field strength, image acquisition time, spatial resolution, signal-to-noise ratio (SNR), and motion artifacts. These parameters were chosen based on their direct impact on diagnostic accuracy and usability of MRI systems in both routine and advanced clinical applications. A comparative table (Table 1) was developed to illustrate the performance differences between the two systems, followed by a visual representation of the findings in Figure 1. Measurements were standardized to allow for parallel comparison and to eliminate institutional or manufacturer-specific variability.

In addition, cost evaluation was performed by reviewing current market data, equipment acquisition contracts, and total cost of ownership analyses. Four financial criteria were assessed: initial acquisition cost, annual operational cost, maintenance cost, and software upgrade cost. All values were normalized to

a 10-year lifecycle to ensure comparability and reflect the total investment required for each system type. The results are summarized in Table 2 and visually represented in Figure 2.

To assess image quality performance, four diagnostic dimensions were investigated: structural clarity, tissue contrast, lesion detectability, and image artifacts. This analysis was based on a synthesis of published clinical case studies and benchmarking literature. Figure 3 illustrates a comparative evaluation based on these image quality indicators. Although direct image acquisition was not performed, the indicators were validated using simulation studies and vendor-provided reference datasets.

Throughout the study, efforts were made to maintain objectivity and avoid bias by cross-validating technical data with clinical findings from independent research publications. The approach integrates both quantitative metrics and qualitative expert evaluations, making the findings relevant to radiologists, medical physicists, and hospital procurement officers.

3. Results and discussions

To assess the technical performance and economic feasibility of 1.5 T and 3 T MRI scanners, a comparative analysis was conducted based on documented specifications and operational characteristics. The evaluation covered magnetic field strength, image acquisition time, spatial resolution, signal-to-noise ratio, and artifact susceptibility.

Table 1 summarizes the key technical specifications of MRI systems with magnetic field strengths of 1.5 Tesla and 3 Tesla. The comparison includes magnetic field intensity, image acquisition time, spatial resolution, signal-to-noise ratio (SNR), and the presence of motion artefacts. The data indicate that MRI 3 T scanners provide faster acquisition, higher spatial resolution, improved SNR, and reduced artefacts compared to MRI 1.5 T systems.

Figure 1 highlights key technical differences between MRI scanners operating at 1.5 Tesla and 3 Tesla. The comparison includes magnetic field strength, image acquisition time, spatial resolution, signal-to-noise ratio (SNR), and motion-related artefacts. MRI 3 T outperforms MRI 1.5 T in most parameters, offering faster imaging, better resolution, higher SNR, and fewer artefacts, making it more suitable for advanced diagnostics.

In terms of operational economics, cost remains a decisive factor in institutional acquisition. The initial purchase cost and annual maintenance expenses are notably higher for 3T systems. However, this is often offset by their clinical



N°. 3 - 2025, ISSN 2668-4748; e-ISSN 2668-4756 Article DOI: https://doi.org/10.35219/mms.2025.3.01

advantages, particularly in high-throughput facilities or specialized diagnostic centres.

Table 2 presents a financial overview of MRI systems, comparing 1.5 T and 3 T models in terms of initial purchase price, annual operating costs, maintenance expenses, estimated lifespan, and

software upgrade costs. MRI 3 T systems show significantly higher costs across all categories, reflecting their enhanced capabilities. However, MRI 1.5 T units remain a financially viable solution for standard clinical applications.

Table 1. Technical Parameter Comparison between MRI 1.5 T and MRI 3 T

Parameter	1.5 T MRI	3 T MRI
Magnetic field strength (Tesla)	1.5	3.0
Image acquisition time	20 minutes	15 minutes
Spatial resolution	Medium	High
Signal-to-noise ratio (SNR)	50:1	80:1
Motion artifacts and distortions	Medium	Low

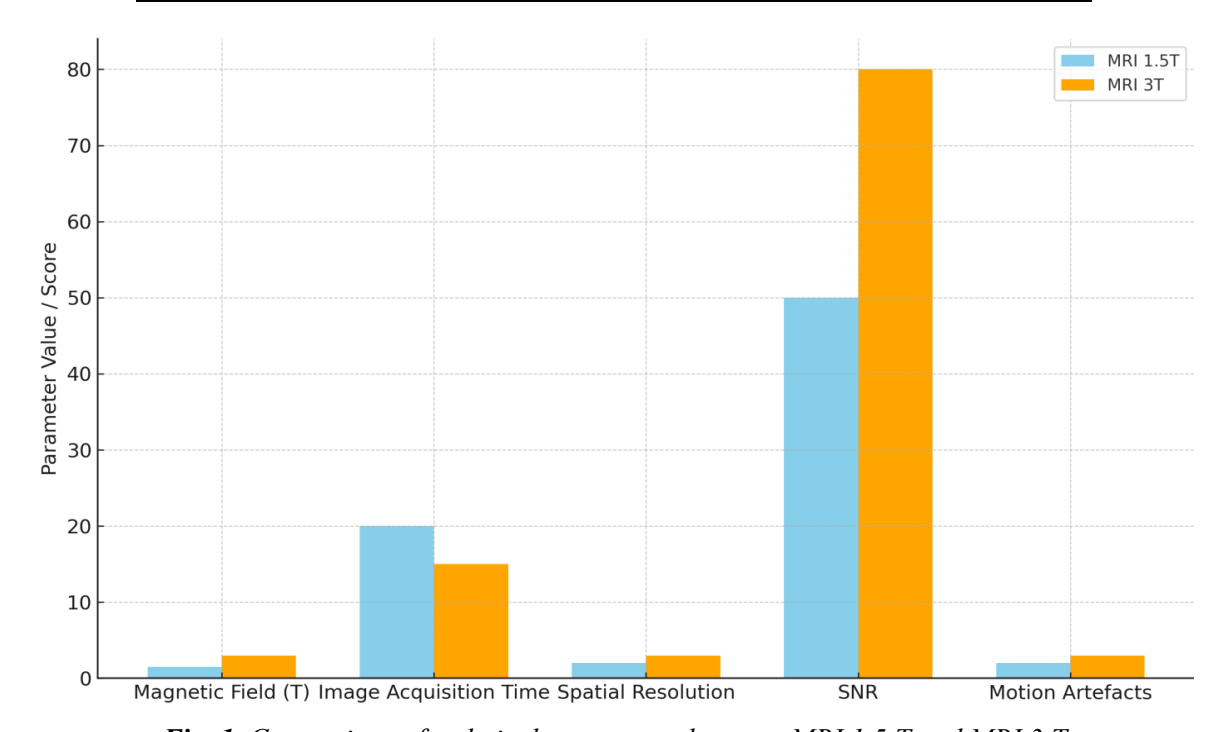


Fig. 1. Comparison of technical parameters between MRI 1.5 T and MRI 3 T

Table 2. Cost Comparison between MRI 1.5 T and MRI 3 T

Cost Category	1.5 T MRI	3 T MRI
Initial purchase cost	\$1,000,000	\$1,500,000
Annual operating costs	\$100,000	\$150,000
Annual maintenance costs	\$50,000	\$75,000
Software upgrade costs	\$10,000	\$15,000
Estimated lifespan	10 years	10 years



N°. 3 - 2025, ISSN 2668-4748; e-ISSN 2668-4756

Article DOI: https://doi.org/10.35219/mms.2025.3.01

Figure 2 illustrates the significant financial investment required for 3 T MRI systems. Despite higher costs, the improved image quality and reduced scan time can translate into higher diagnostic accuracy and increased patient throughput, which may justify the investment in specific clinical contexts.

In addition, the quality of imaging was further evaluated based on clarity, tissue contrast, lesion detectability, and artifact suppression. The 3 T MRI consistently outperformed the 1.5 T MRI across all criteria, offering better contrast, higher detail visibility, and lower susceptibility to motion-related artifacts.

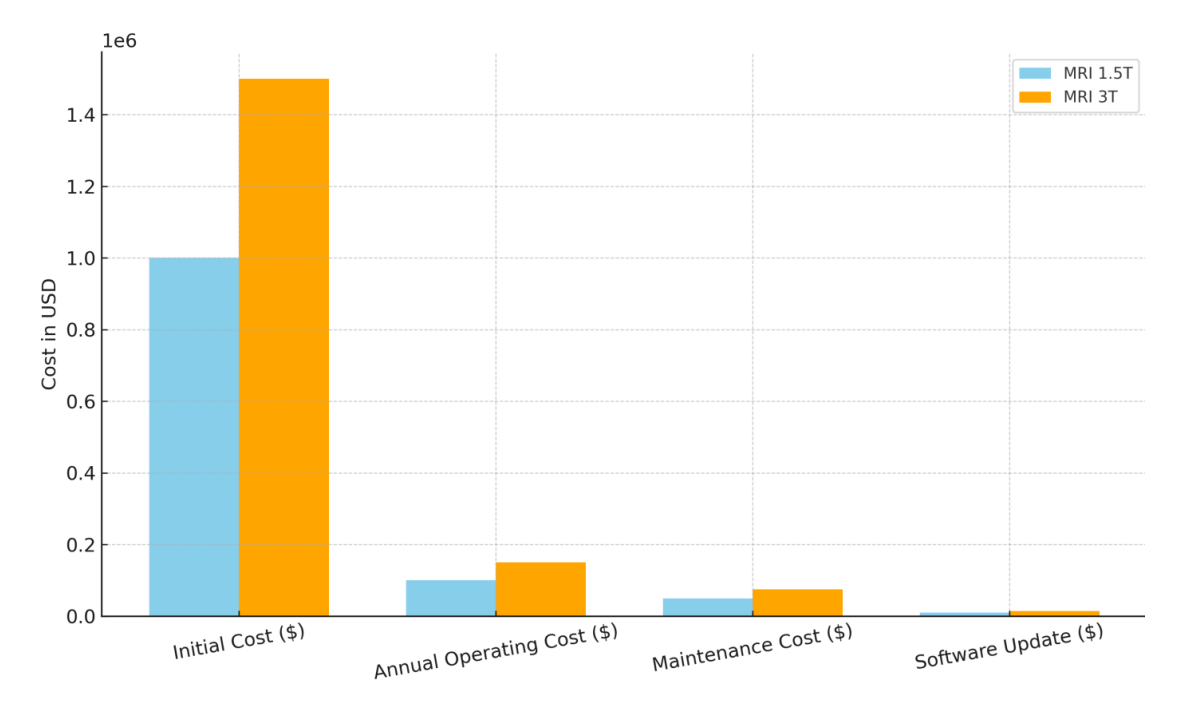


Fig. 2. Cost comparison between MRI 1.5 T and MRI 3 T

Figure 3 illustrates the comparative evaluation of image quality parameters for MRI scanners with 1.5 Tesla and 3 Tesla magnetic field strengths. The analysis covers four key criteria: structural clarity, tissue contrast, small lesion detection, and presence of

image artefacts. MRI 3 T consistently outperforms MRI 1.5 T, demonstrating superior clarity, enhanced contrast, and improved lesion visibility, while also reducing artefacts, making it more suitable for advanced diagnostic imaging.

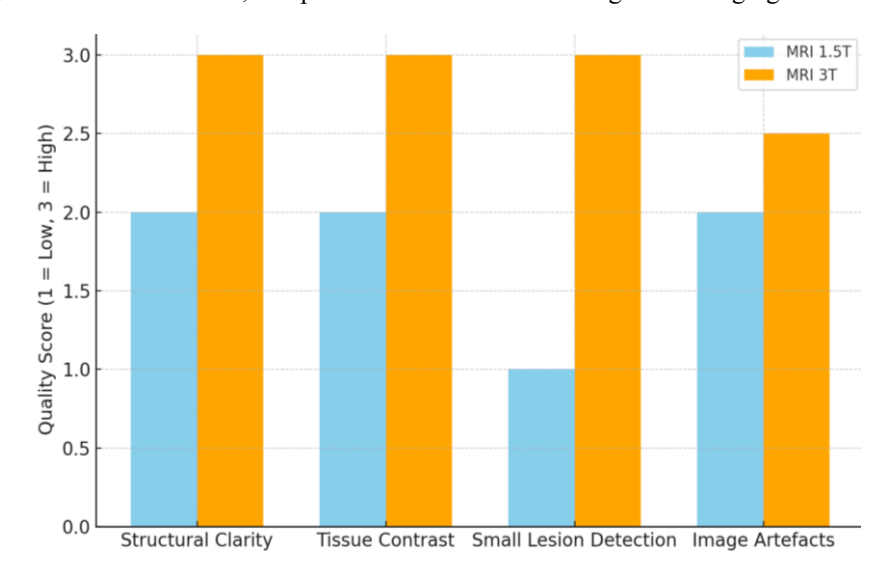


Fig. 3. Comparison of image quality parameters between MRI 1.5 T and MRI 3 T



N°. 3 - 2025, ISSN 2668-4748; e-ISSN 2668-4756

Article DOI: https://doi.org/10.35219/mms.2025.3.01

4. Conclusions

This comparative analysis of 1.5 T and 3 T MRI systems highlight significant technical and economic differences between the two modalities. From a technical standpoint, the 3 T MRI system consistently demonstrates superior spatial resolution, higher signal-to-noise ratio, reduced acquisition time, and fewer motion artifacts, making it more suitable for complex and high-precision diagnostic applications. In contrast, the 1.5 T MRI remains a cost-effective and clinically viable solution for routine examinations, with acceptable imaging quality for general diagnostics.

Economically, the 1.5 T system presents clear advantages in terms of lower initial acquisition costs, maintenance, and operational expenses, which may be decisive for smaller medical centres. However, the higher upfront investment in 3 T MRI systems can be justified in institutions where high image quality, advanced neurological, musculoskeletal, or oncological assessments are frequently required.

The evaluation of image quality further reinforces the technical superiority of 3 T MRI, particularly in detecting subtle pathologies and delivering improved tissue contrast. Nevertheless, both systems have their place in clinical practice, and the choice should be based on the specific diagnostic needs, patient population, and financial capacity of the institution.

Future work should focus on the integration of AI-based post-processing tools and deep learning algorithms that could enhance the performance of both 1.5 T and 3 T systems, potentially reduce the

current technical gap and optimize resource allocation in medical imaging services.

References

- [1]. Wu M., Zhang L., Li C., 3 T vs 1.5 T MRI: the good, the bad and the ugly, Insights into Imaging, vol. 12, p. 113, 2021.
- [2]. Wiersma H. W., Weber M. A., Cost-effectiveness of 3 T MRI versus 1.5 T in knee imaging, RöFo Fortschr. Röntgenstr., vol. 190, no. 3, p. 272-279, 2020.
- [3]. Potter K. A., Matson M. B., 1.5 T vs 3 T MRI: clinical implications, Investigative Radiology, vol. 56, no. 11, 2021.
- [4]. Radiopaedia Contributors, 1.5 T vs 3 T MRI: technical comparison, Radiopaedia, 2021.
- [5]. Taylor C. M., Nguyen D., Comparison of diagnostic performance of brain MRI at 1.5 T vs 3 T, Am. J. Roentgenol., vol. 221, no. 1, p. 45-52, 2023.
- [6]. Costantino L., Schmidt N., Economic viability of 3 T MRI in oncology centers, J. Clin. Neurosci., vol. 102, p. 134-139, 2023.
- [7]. Liao B., Chen Y., Wang Z., A comparative study on 1.5 T-3 T MRI conversion through deep neural network, arXiv preprint, 2022.
- [8]. Iglesias J. E., Billot B., Accurate super-resolution low-field brain MRI, arXiv preprint, 2022.
- [9]. Kaur P., Minhas A. S., Ahuja C. K., Estimation of 3 T MR images from 1.5 T images, arXiv preprint, 2024.
- [10]. Chakravarty A., Debnath J., Life cycle costing of MRI machine, J. Clin. Imaging Sci., vol. 10, p. 81, 2020.
- [11]. Ezra Medical, 3 T vs 1.5 T MRI: how do they compare?, Ezra Medical Blog, 2023.
- [12]. RITE Advantage, MRI 1.5 T vs 3.0 T what is the difference?, RITE Clinical Education, 2022.
- [13]. Mahajan A., Raman S., Cost-effectiveness of specialized MRI for dizziness, Am. J. Roentgenol., vol. 221, no. 4, 2023.
- [14]. Pisch R., Becker C. R., Comparison of abdominal imaging at 1.5 T vs 3 T, Radiographics, vol. 41, no. 3, p. 741-758, 2021.
- [15]. Vilanova J. C., Low-field vs high-field MRI: cost-effectiveness study, Eur. Soc. Radiol. Conf. Proc., 2025.
- [16]. Radiopaedia Contributors, 1.5 T vs 3 T MRI: artifact and SNR considerations, Radiopaedia, 2021.



N°. 3 - 2025, ISSN 2668-4748; e-ISSN 2668-4756 Article DOI: https://doi.org/10.35219/mms.2025.3.02

RESEARCH ON CREATING DECORATIVE OBJECTS FROM GLASS WASTE THROUGH THERMOFORMING

Beatrice Daniela TUDOR

"Dunarea de Jos" University of Galati, Romania e-mail: batrice.tudor@ugal.ro

ABSTRACT

The paper presents a research study on the production of decorative glass objects using the thermoforming process. For this purpose, glass waste was used, aiming at the recovery and reuse of various glass scraps for the production of ornamental objects. The thermoforming process was applied to various combinations of white and coloured glass with inserts from different materials to achieve the most pleasant visual impact, producing different shapes and geometries.

KEYWORDS: glass, thermoforming, decorative objects, waste

1. Introduction

Decorative glass elements have become a symbol of elegance and sophistication in modern interior design. The role of decorative glass elements in luxury design is significant. Glass adds a modern look, reflecting light and creating a feeling of open space. It can be used to highlight design elements, such as furniture or works of art.

Each type of glass has its own unique characteristics, which can be exploited to create a special interior design, both by using decorative art objects and by incorporating glass into lighting fixtures or building elements, such as decorative walls, windows, and doors [1, 3].

Decorative objects can be made from glass waste through various methods, transforming used glass into unique and attractive pieces. Recycling glass is a sustainable option, and the process can be customized to create various decorative objects.

There are numerous possibilities to transform glass waste into decorative objects, contributing to environmental protection and the creation of unique and valuable pieces.

Every time we produce new bottles, we need materials from coastal areas, where soil erosion is a real problem. The more we produce new items, the more sand we take from these areas. Therefore, one way we can contribute to protecting the environment is to reuse the materials, through "upcycling" and by creating personalized decorative objects [2].

2. Experimental research

To obtain ornamental pieces by thermoforming, I made several attempts, on different combinations of glass waste with different inserts. I used refractory brick as a template, on the surface of which I placed different pebbles to ensure, through them, convex deformations of various shapes and sizes.

Between the pebbles and the refractory brick, I placed a ceramic separator, and over the pebbles, a coloured glass plate. For this study, I used glass waste

We followed the behavior of the glass during the thermoforming cycle. In addition to the uneven heating provided by the oven, there were also sudden temperature variations, as a result of repeated openings of the oven door, which ultimately led to the appearance of stresses inside the glass sheet and, subsequently, to the appearance of cracks and fissures.

Figure 1 shows the assembly, sheet-pattern, fixed on the refractory brick, which was inserted into the oven.

The refractory support ensured, when the assembly was introduced into the furnace, the preservation of the chosen design and reduced the temperature variations that usually occur along the height of the furnace.

Figure 2 shows the ornamental object obtained after thermoforming.

You can see the cracks that appeared in the glass sheet - specifically, the cracks at the level of the bulge, in the upper part of the deformed glass (Figure 3), as well as the cracks that led to the delimitation of



N°. 3 - 2025, ISSN 2668-4748; e-ISSN 2668-4756

Article DOI: https://doi.org/10.35219/mms.2025.3.02

fragments of smaller or larger sizes; practically, pieces detached (broken off) from the glass sheet.

The pebbles with variable sizes and large differences in height, together with the temperature variations caused by the oven and those "introduced" due to the door opening, led to the compromise of the first "thermoformed" decorative object.

The convexity of the glass, its varied height and its asymmetrical positioning - all influenced by the pebbles - proved that the method can lead to the creation of interesting decorative objects.

An important problem with this piece is the imprints of the pattern left on the piece (Figure 4.). The texture given by the separator is also visible on the edge of the sample.



Fig. 1. Model assembly, glass sheet-pebbles



Fig. 2. Thermoformed ornamental object



Fig. 3. Superficial cracks on the surface of the part



N°. 3 - 2025, ISSN 2668-4748; e-ISSN 2668-4756

Article DOI: https://doi.org/10.35219/mms.2025.3.02



Fig. 4. Imprinting of pebbles on the surface of the piece

In the next sample taken into the study (Figure 5), we used smaller, more uniform pebbles, without too many temperature variations in the working space of the furnace induced by the outside, and better results were obtained.



Fig. 5. Decorative ensemble made of brown glass (ornament) and thermoformed pebbles



Fig. 6. Texture of the thermoformed sample, due to the shape of the pebbles

When removed from the oven, the transformed plate, with the protuberance given by the pebbles used as a model, presented a slight transverse crack,

which over time propagated, transforming into a much larger one. Due to the shape of the pebbles with inclinations in both directions, some of them remained trapped in the piece, and their final detachment from the respective areas damaged the object.

It is worth mentioning that the crack appeared in approximately the same area, observed in all samples taken, located in an area with greater temperature variations, recorded along the length of the furnace.

Another test consisted of combining two types of glass, with different colours, which we assumed could have the same expansion coefficient, being the case of window glass with a printed pattern from the factory.

To create the assembly (Figure 7), in addition to the two types of coloured glass, out of the desire to print a more unique pattern on the support glass, we also placed some wires, with a diameter of 3 mm, between it and the ceramic separator.



Fig. 7. The combination of the two types of glass, with different colours, placed on steel wires

The plate obtained (Figure 8) confirmed the assumption that the two types of glass have the same or a similar coefficient of expansion, as there was good compatibility between them. And in this case, in the area with temperature variations, a slight crack



N°. 3 - 2025, ISSN 2668-4748; e-ISSN 2668-4756

Article DOI: https://doi.org/10.35219/mms.2025.3.02

appeared which over time led to cracking and breaking.

Here, as in the previous case, some pieces of wire, like pebbles, remained embedded in the plate, but they could be extracted. A possible cause of the crack can also be considered the lack of compatibility between the glass and the metals used to obtain the ornamental motif.



Fig. 8. Thermoformed assembly, made of brown glass, green glass, wire strands

To see the behavior of the two types of factory-decorated glass and transparent window glass, we created an assembly consisting of three different layers: a transparent glass plate as the background support, brown decorative glass (wavy type) in the middle, and on top, green decorative glass with a geometric ornament.

However, some defects were also observed, but these cannot be attributed to the existence of several types of glass and their different thermal expansion coefficients.

As can be seen from Figure 9, due to the dimensions of the base glass plate, which exceeded those of the refractory brick, when the glass softened, it flowed past the edges of the brick, giving rise to several fringes, almost perpendicular to the support plate.



Fig. 9. Ornamental shape made of three types of glass (brown, green, transparent) thermoformed

The missing portion at one of the ends is explained by the fact that it was located in the area of the highest temperatures, at the back of the furnace.

At the working temperature, 800 °C, the thermoforming temperature, the glass became less viscous, and the oversized portions, softening, took the shape of the brick, molded on the edge and elongated, and under their own weight, they broke. The missing portion was formed, according to the drawing, of two layers of glass, therefore slightly heavier.

No cracks were recorded, so the three types of glass may have had equal expansion coefficients or only small variations between them.

Based on these results, I also wanted to create some decorative objects, slightly more special, made of overlapping coloured glass bars.

The first of them (Figure 10) was made only of glass bars of a single colour (brown), compatible with each other.



Fig. 10. Decorative object made of overlapping glass bars

Maintaining the piece for a longer time at the final temperature of 800 °C led to the perfect joining of the bars and to the creation of a decorative object without cracks (Figure 11a). The texture, given by the ceramic separator and the non-uniformities of the brick, can be observed in Figure 11b.

In the second decorative object made, difficulties arose in preserving its design, not through the alternation of colours, but through the dimensions, the spaces between the bars and their positioning. The great weight of the entire assembly, formed by the brown and green glass strips and the brick, its cumbersome handling (pushing it onto the hearth of the oven until it touched the back wall), combined with the gloss of the glass and the reduced space of the oven enclosure, led to the displacement of the strips, resulting in the deterioration of the geometry.

Following the same conditions as in the previous case, we obtained a second decorative object, two-coloured (Figures 12a and b), without cracks or thermoforming defects.



N°. 3 - 2025, ISSN 2668-4748; e-ISSN 2668-4756

Article DOI: https://doi.org/10.35219/mms.2025.3.02

The small irregularities that appear on the back of the pieces or certain sharper corners or curves that appear at the edges can be explained by the fact that the strips exceed the refractory brick surface in some areas, which caused the appearance of deviations from the general shape of the strips at some edges [4, 6].





Fig. 11. Decorative object made of thermoformed glass bars: a) thermoformed object; b) its texture

It is also worth mentioning that on the back of the object created, such as compact plates or lattice plates, the texture of the support used as a separator was imprinted, to prevent the glass from sticking to the refractory material (Figure 12). As objects of comparison, I took a similar one, obtained in two different workshops: a workshop in Brăila (Figure 13b), and another obtained in a workshop abroad (Figure 13c), next to which I placed one of the decorative objects created by me (Figure 13a).





Fig. 12. Thermoformed objects from bicolour glass bars; a) thermoformed object; b) texture

I also made an object, not necessarily decorative, but more useful, such as a small glass ashtray, obtained towards the end of the study, when I

considered that I could improvise and control the thermoforming process.



N°. 3 - 2025, ISSN 2668-4748; e-ISSN 2668-4756

Article DOI: https://doi.org/10.35219/mms.2025.3.02

I used a truncated metal cone, not too large (Figure 14), with which I obtained the hole in the glass sheet.

The glass plate was in the form of a circle, with a radius of approximately 120 mm, shaped according to the diameter of the bottom, the height of the walls, and the outer border. To prevent the glass from being imprinted by the metal mould and the refractory brick, we used a separator in the form of a powder of ceramic particles, with which, after soaking in water, we coated the parts that the glass was to come into contact during thermoforming. On the refractory brick and in the mould, we placed a ceramic separator [5].

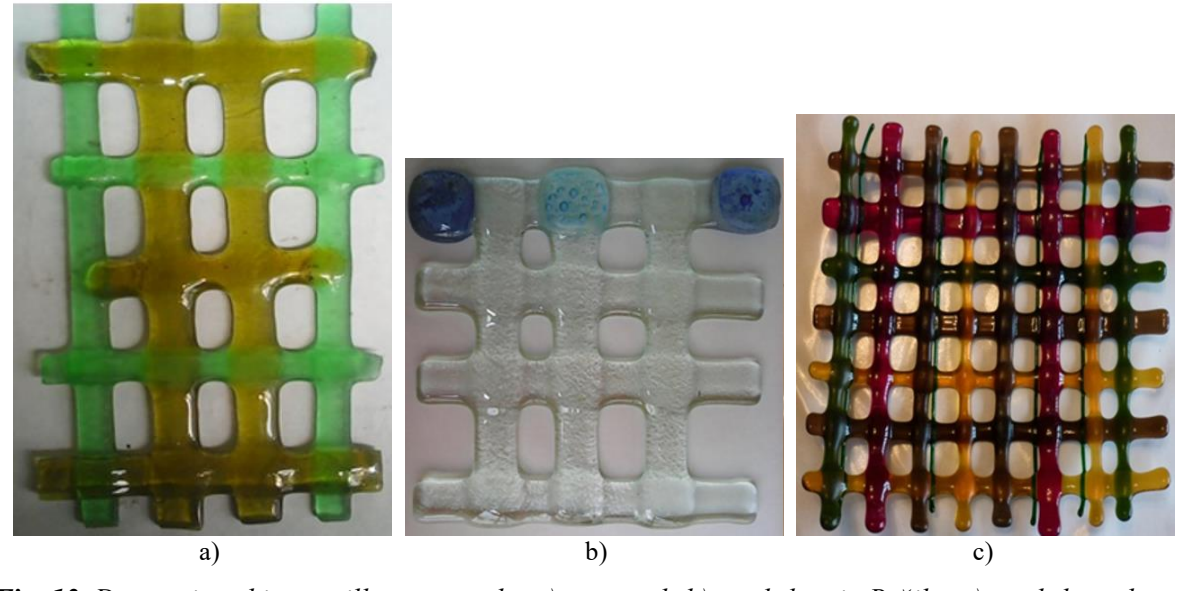


Fig. 13. Decorative object, grille type, made: a) personal; b) workshop in Brăila; c) workshop abroad

The final product, a small ashtray (Figure 15), exhibited the same defects caused by uneven heating and improper shapes:

- copying of shape defects;

- diametrically opposed areas of the walls of the inner cylinder of the ashtray with different heights;
- asymmetries in the marginal border.





Fig. 14. Metal support for thermoforming the ashtray: a-cleaned metal support before thermoforming; b-metal support after thermoforming



N°. 3 - 2025, ISSN 2668-4748; e-ISSN 2668-4756

Article DOI: https://doi.org/10.35219/mms.2025.3.02





Fig. 15. Thermoformed glass ashtray

3. Conclusions

The study and research conducted led to the conclusion that glass waste can be transformed into unique and personalized decorative objects.

Research conducted on different samples, with various inserts and geometries, highlighted the importance of temperature and the thermal expansion coefficient on the viscosity of glass.

Through creative recycling, also known as creative reuse, new products of higher quality or value are created.

The advantages of using recycled glass to make decorative objects are: sustainability, creativity and originality. The objects created have a unique and personalized look.

References

- [1]. James L. Throne, *Understanding Thermoforming 2E*, 2nd Edition, Hanser Publications, ISBN-10:1569904286, ISBN-13:978-1569904282, May 8, 2008.
- [2]. Florea Gh., Chiriac Al., Mărginean I., Procedee performante de punere în formă, partea I, Editura Europlus, Galați, 2008.
- [3]. James L. Throne, Technology of Thermoforming, Hanser Publications, ISBN-10:1569901988, ISBN-13:978-1569901984, July 18, 1996.
- [4]. Mohácsi Renáta, Obiecte vopsite din sticla, Editura Casa, ISBN: 978963966573, 2009.
- [5]. ****, https://chemcast.com.mx/img/pdf/Fabrication_manual_thermoform ing.pdf.
- [6]. ***, https://www.sciencedirect.com/topics/materials-science/thermoforming-process.



N°. 3 - 2025, ISSN 2668-4748; e-ISSN 2668-4756

Article DOI: https://doi.org/10.35219/mms.2025.3.03

STUDIES AND RESEARCH ON **OBTAINING GLASS INLAYS IN METAL**

Beatrice Daniela TUDOR

"Dunarea de Jos" University of Galati, Romania e-mail: batrice.tudor@ugal.ro

ABSTRACT

The paper presents research on obtaining glass inlays in metal, with the aim of obtaining a decorative object, using the intarsia technique. For this purpose, we studied the samples that we made from glass shards of different sizes, over which different metal oxides were added to colour the glass. The samples were made with different amounts of metal oxide, respectively 4%, 7%, and 10% to obtain different shades of colour. We also conducted experimental research to achieve the embedding of some pieces of glass in a defined metallic contour. The decorative object was made through the thermoforming process, with the glass intarsia in metal, in a stainless-steel plate, used as a background.

KEYWORDS: intarsia, glass, design, metal, thermoforming

1. Introduction

Thermoformed glass is becoming increasingly well-known and sought after, especially among architects and designers. Thermoformed glass is created by fusing glass of different shapes and colours. Products made from thermoformed glass are considered unique items.

Thermoformed glass can be used with confidence, both indoors to create various decorative objects, and outdoors in place of classic windows, by replacing them with personalized stained glass. The major advantages of thermoformed glass are the ingredients used, which differ from one product to another, and thanks to the technology used, stained glass is considered to be a resistant, durable and easyto-maintain material.

Intarsia is an artisanal marquetry technique that involves inlaying small pieces of different materials on a surface. Traditionally, this technique uses wood, but it can be transferred to other materials. Intarsia requires precision and meticulous cutting of the pieces to create complex and varied designs [1, 3].

2. Experimental research

One of the objectives of the study was the production of decorative intarsia-type objects. The first experiments were carried out in the direction of obtaining the embedding of pieces of glass in a determined metallic contour. The frames were

obtained by welding, side by side, separate pieces of steel sheet. They did not have a perfectly delimited surface, and the material used showed strong oxidation tendencies. Some of the shapes used are shown in Figure 1.



Fig. 1. Metal frames used for the study of glass embedding inside them

The flat pieces of glass were cut to dimensions as close as possible to the inner contour of the frames, and where there were deviations from their configuration, they were removed by grinding. Some of the frames prepared for the study are shown in Figure 2.

The samples obtained could not ensure a good fit between the inner walls of the frame cavity (Figure



N°. 3 - 2025, ISSN 2668-4748; e-ISSN 2668-4756

Article DOI: https://doi.org/10.35219/mms.2025.3.03

3). This is necessary when inlaying the glass in metal, which replaces adhesive bonding.



Fig. 2. Frames with glass plates inside

I also analysed the possibility of using pieces of glass slightly larger than the size of the mould (round samples), aiming to see if, through thermoforming, the desired relief could be obtained, by deforming the glass under its own weight (so that the glass plate rests on the edges of the mould) and falls inside the mould, thus perfectly occupying the inner surface of the mould.

The test results can be seen in Figure 4b.

The glass used for the two samples was cut differently; for the larger diameter sample, a diamond cutting tool was used, and for the smaller sample, the disk was obtained by carving the piece of glass with special pliers. The impossibility of obtaining glass contours as close as possible to the dimensions of the

shape led to the use of shredded glass, which, by heating at higher temperatures, resulted in obtaining the exact configuration of the metal cutouts.

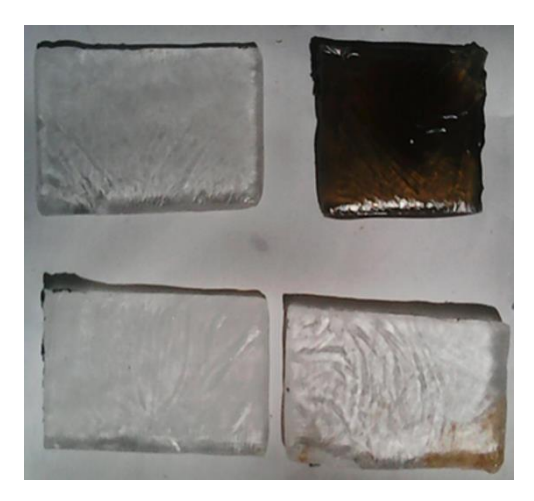


Fig. 3. Samples after removal from the oven

This option also offered the possibility of colouring the glass, to obtain the decorative object.

I made the samples with glass shards of different sizes, over which I added different metal oxides, with which I coloured the glass.

Coloured glass is obtained by adding quantities of iron, copper, nickel, silver, gold or other metal combinations. In this way, almost infinitely many colour variations can be obtained [2, 4].



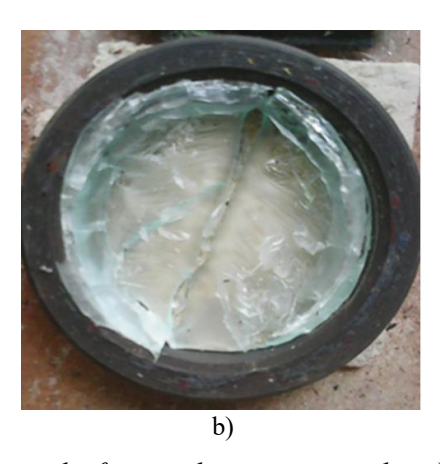


Fig. 4. Sample for the study of glass embedding in the form under its own weight: a) sample preparation; b) thermoformed sample

For example, red glass contains copper oxide, yellow glass contains cadmium sulphate, blue glass contains cobalt oxide, green glass contains chromium oxide, and violet glass contains manganese oxide.

After studying the samples, we observed that on larger shards, the adhesion of the dye was lower,

resulting in incomplete colouring due to the difference in melting temperature between the two components (Figure 5), leaving the outline of the shards highlighted by oxides visible.

The very small shards trapped the metal oxides between them, leading to uniform colouring. We



N°. 3 - 2025, ISSN 2668-4748; e-ISSN 2668-4756

Article DOI: https://doi.org/10.35219/mms.2025.3.03

made samples in which, in the very fine glass fragments, we introduced 4, 7 and 10% metal oxides. We used shards from green and brown bottles, obtained from bottles of these colours (Figure 6).

The top row shows samples with green glass; the bottom row shows samples with brown glass.

For the green glass powder, we used the addition of green chromium oxide, and for the brown glass, yellow iron oxide.



Fig. 5. Staining sample with glass shards and metal oxides

It was found that in the samples with 4% oxide (Figure 7 a), the powder and oxide gave rise to a glass with different colour intensities than those of the standard samples, which originated only from fine glass powder of the same green and brown colour, respectively, and with characteristics close to those of glass (such as gloss and smoothness).

In the samples obtained with the addition of 7% oxide (Figure 7b), the colour intensity of the two samples increased. Instead, their appearance diverged from that of glass, losing smoothness and gloss.

In the sample with 10% oxide addition (Figure 7c), a change in the colour intensity of the samples is observed, and the appearance, lacking smoothness and gloss, is very close to that of grindstones.

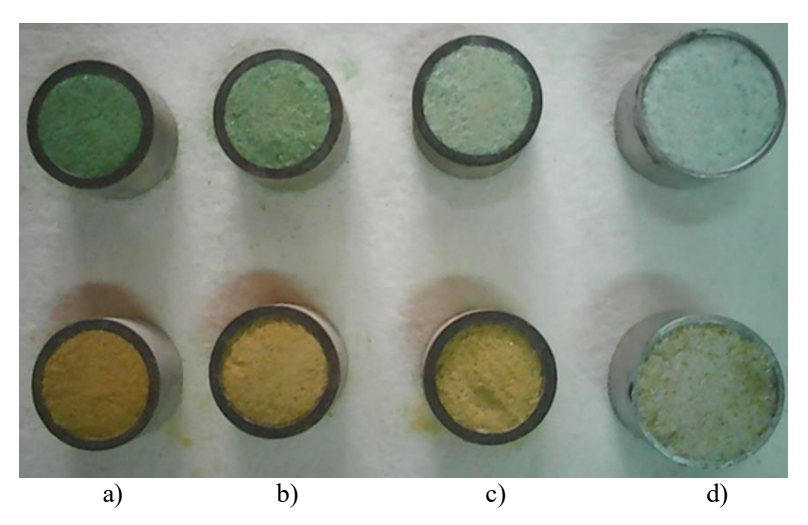


Fig. 6. Rings with mixtures of glass and oxides prepared for treatment: a- powdered glass with 10% oxide; b) powdered glass with 7% oxide; b) powdered glass with 4% oxide; d) powdered glass colour standard

Due to the characteristics of the surface and the resulting colours for subsequent processing operations of glass waste, the most suitable materials

are mixtures made only from glass powder, or from glass powder with a maximum of 7% oxide addition.

For special ornamental effects, mixtures obtained with an addition of 10% oxide can also be



N°. 3 - 2025, ISSN 2668-4748; e-ISSN 2668-4756

Article DOI: https://doi.org/10.35219/mms.2025.3.03

used. The final product differs from the initial, monochromatic powder by its rough appearance and the stronger intensity of the colours.

In the research carried out, I proposed creating a small painting using the intarsia of some pieces of glass in a metal base plate. When creating the decorative object, because some elements could not be cut from glass, I resorted to the help of glass powder, to obtain them.

The drawing of the painting that I proposed to "paint" by thermoforming is the one presented in Figure 8.

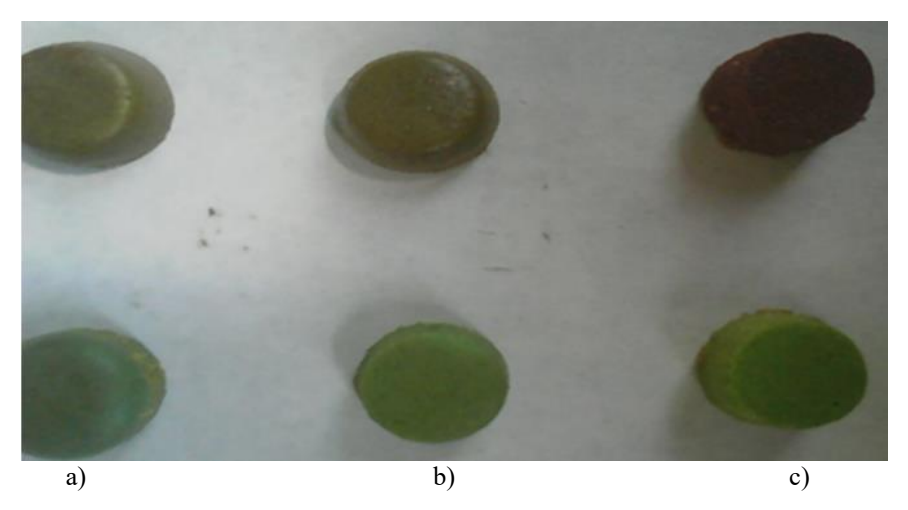


Fig. 7. Samples obtained: a) with 4% addition; b) with 7% addition; c) with 10% addition

We opted for a stainless-steel sheet as the background, and inlays obtained in two ways, respectively: cut glass and powdered glass. The sheet of metal was sectioned into several pieces, processed by grinding, and, finally, the plate was reconstituted by welding (Figure 9).

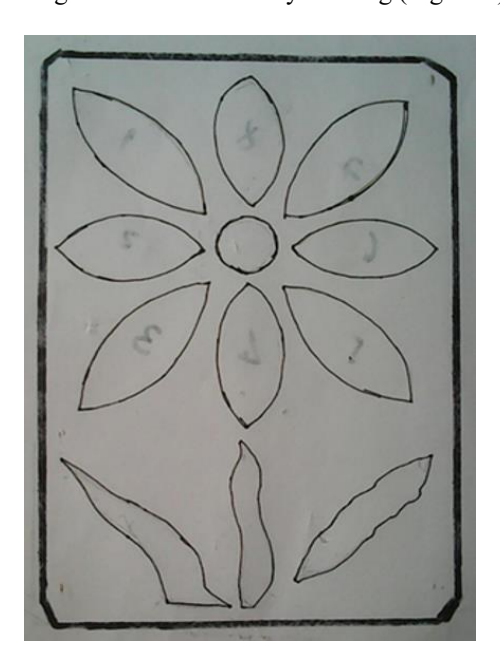


Fig. 8. Drawing of the painting, with glass inlay in metal

The glass inlays, such as the petals, were quite difficult to make (Figure 10).

To ensure the fixation (embedding) of the glass in the metal plate, between the two components, sheet metal and glass, we introduced fine glass powder, which, by softening at the same time as the glass, ensures the best possible connection of the glass elements with the metal base plate (Figure 11).

The small elements, such as leaves, were made of fine glass powder (Figure 11). The thickness of the powder layer was twice the thickness of the 2 mm plate, because during thermoforming the layer loses



N°. 3 - 2025, ISSN 2668-4748; e-ISSN 2668-4756

Article DOI: https://doi.org/10.35219/mms.2025.3.03

its height, and the desired relief can no longer be achieved. After thermoforming, cooling was done together with the oven, to ambient temperature [5].

The central area of the flower was modeled by placing a the ceramic separator, fixed, in turn, on the support plate of the entire assembly, with a thin piece of white glass, then coloured by covering it with larger fragments, also from glass of the same quality and colour.

The decorative object obtained, upon removal from the oven, is shown in Figure 12.

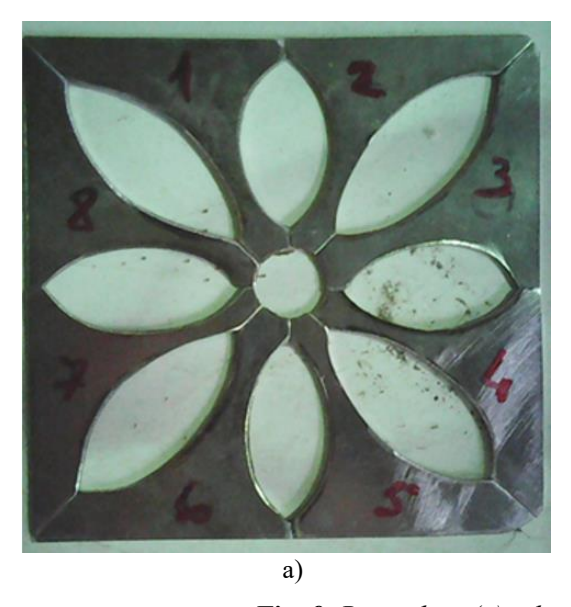




Fig. 9. Base plate (a), plate after assembly (b)



Fig. 10. The base plate and inlays in the process of formation



Fig. 11. Preparation of the plate-inlay assembly for thermoforming



N°. 3 - 2025, ISSN 2668-4748; e-ISSN 2668-4756

Article DOI: https://doi.org/10.35219/mms.2025.3.03



Fig. 12. Decorative object made by inlaying glass in metal (stainless steel) through thermoforming

4. Conclusions

Intarsia is an artisanal marquetry technique that involves inlaying small pieces of different materials onto a surface. Traditionally, this technique uses wood, but it can be transferred to other materials. Intarsia requires precision and meticulous cutting of the pieces to create complex and varied designs.

The decorative object was made through the thermoforming process and the inlay of glass in metal, in a stainless-steel plate, used as a background.

We also conducted experimental research to obtain the embedding of glass pieces in a determined metallic contour.

Following various attempts, a unique and personalized decorative object was created by inlaying glass in metal through thermoforming.

References

[1]. Karen L. Cohen, Art of Fine Enameling, Editura Stackpole Books, ISBN 9780811737920, 2020.

[2]. Carole Ferrer, *Vitralii-2014*, Cod: MAS978-973-1822-99-0, Editura: MAST, 2014.

[3]. Kathy Wise, Intarsia: Woodworking Projects [With Patterns], Editura: Fox Chapel Publishing, ISBN 1565233395, 2007.

[4]. Kathy Wise, Intarsia Woodworking for Beginners: Skill-building Lessons for Creating Beautiful Wood Mosaics, Fox Chapel Publishing, 2009.

[5]. Florea Gh., Chiriac Al., Mărginean I., Procedee performante de punere în formă, partea I, Editura Europlus, Galați, 2008.



N°. 3 - 2025, ISSN 2668-4748; e-ISSN 2668-4756 Article DOI: https://doi.org/10.35219/mms.2025.3.04

HOW BLOCKCHAIN CAN RESHAPE THE SUPPLY CHAIN OF STEEL FOR AN INDUSTRIAL COMPLEX

Ștefănică FRANGU, Ioan ȘUȘNEA

"Dunărea de Jos" University of Galați, Romania e-mail: frangu.stefanica@gmail.com, ioan.susnea@ugal.ro

ABSTRACT

Steel is an integral part of modern infrastructure and is present in buildings, vehicles, and machinery. Although ubiquitous, the process of converting raw materials into usable products is highly advanced and, in almost all instances, largely unseen. Blockchain can ensure secure, transparent ledgers are maintained throughout each step of the process, from mining and processing to production and export. This enables companies to verify the origin of the steel, the processes undertaken during its production, and its conformity to safety and environmental standards.

This article demonstrates how blockchain is transforming the steel sector by accelerating, simplifying, and making the tracking process more environmentally friendly. It presents the advantages and disadvantages of applying digital technology to traditionally analogue businesses, based on real-world cases and research.

Readers will learn how a conventional business, with a history spanning centuries, is beginning to capitalize on digital opportunities - whether in manufacturing, IT, or even in industrial processes - making it especially relevant to those passionate about technology.

KEYWORDS: steel, blockchain, supply chain, transparency

1. Introduction

The steel producing industrial complex from Galați (Figure 1), one of the foremost integrated steel manufacturers in Europe, has extensive inventories of semi-finished and finished steel products, such as coils, rebar, and structural profiles. It supplies these products to downstream consumers such as construction, automotive, and infrastructure industries.



Fig. 1. Steel-producing industrial complex [1]

To date, the steel-producing industrial complex in Galați has supplied heavy plates for significant infrastructure projects, including: the Railway Bridge for Otopeni Airport—providing over 1,500 meters of plates for the new railway bridge between Bucharest North Station and Otopeni Airport, which enhances national transportation infrastructure [3]; the Danube Bridge at Brăila, which will be the third largest in Europe [2]; the bridges over Mureş River that are part of the A10 Sebeş – Turda motorway; and the "Osman Gazi" Bridge in Turkey [2].

To enhance traceability, regulatory compliance, and customer trust, a blockchain solution is proposed. This initiative covers part of the steel supply chain, ensuring auditable integrity of data from the production to delivery and creating value to the stakeholders who rely on authentic certification, origin traceability, and Environmental, Social, Governance (ESG) reporting.

While technological advancements have improved the manufacturing process, supply chain coordination still depends on outdated systems, fragmented databases, and a lack of transparency.



N°. 3 - 2025, ISSN 2668-4748; e-ISSN 2668-4756

Article DOI: https://doi.org/10.35219/mms.2025.3.04

In contrast with markets targeting consumers, where blockchain adoption is going mainstream, the steel industrial environment comes with its own set of challenges: granularity of data, synchronization of physical to digital, and conservatism of established infrastructures.

2. Benefits of using blockchain

Blockchain is a distributed ledger, shared among all network participants, where all information can be seen in real time without concerns about the data being altered [4].

Major advantages of the application of blockchain in the steel supply chain are:

Transparency

Anyone can view the blockchain ledger and anyone can take advantage of it. Everyone can see the ledger's changes in real time. Process transparency brings trust, making it more difficult to falsify information.

· Security and Immutability

Every block of a blockchain is also safely attached to the previous block, making data manipulation almost impossible to achieve undetected. Once data is irrevocably recorded, it cannot be changed unless the entire network concurs. Blockchain can't be easily hacked and modified due to the fact that it can't be modified.

Decentralization

While classical systems depend upon a central authority, blockchain does not. It decentralizes the authority among a collection of nodes, removing single points of failure and the necessity of intermediaries. It promotes resilience, efficiency, and added system integrity.

• Traceability

With blockchain, these assets, data, or transactions can be tracked real-time throughout their lifecycle. It becomes incredibly vital in the field of supply chain management, as it provides end-to-end

visibility, puts down counterfeiting, and verifies authenticity.

• Efficiency and Speed

When transactions are facilitated through the normal payment systems, it sometimes involves engaging numerous middlemen and also delays. Blockchain makes processes easier as people can make transactions among themselves securely and easily. It minimizes the cost and the time of transactions and operations.

· Cost Reduction

Blockchain helps reduce administrative costs at bay since it becomes less cumbersome to verify, keep track, and settle disagreements among other individuals. It also reduces labour costs associated with manual processes and eliminates errors resulting from manual data entry by enabling smart contracts to handle tasks automatically.

Applications (Figure 2)

Provenance and Traceability: Tracking materials from mines to mills to customers.

Quality Assurance: Recording and validating inspection certificates.

Inventory Management: Real-time tracking of shipments and storage.

Compliance and ESG Reporting: Proving adherence to Environmental, Social, and Governance standards.

Carbon Emissions Monitoring: Measuring and reporting CO₂ emissions across the supply chain and operations for sustainability tracking and regulatory compliance [5].

The implementation includes:

- Digitizing quality and logistics records for each batch of steel.
- Using blockchain to log certifications, production timestamps, and transport milestones.
- Integrating data from IoT sensors to verify temperatures, emissions, and compliance in real-time [6].

These innovations help build customer trust, improve regulatory compliance, and streamline audits.

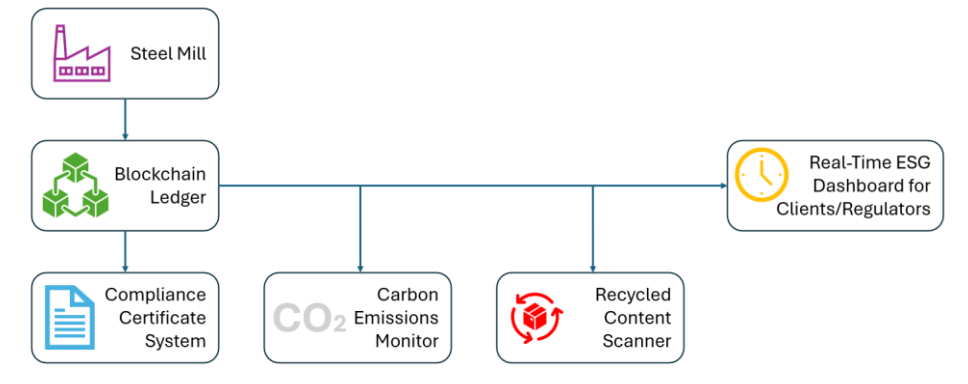


Fig. 2. Blockchain Ledger Applications



N°. 3 - 2025, ISSN 2668-4748; e-ISSN 2668-4756

Article DOI: https://doi.org/10.35219/mms.2025.3.04

Challenges: high initial installation cost, the need for standardization across the industry, resistance to change by current operators, data privacy, and compatibility with legacy systems.

3. Real world use cases

Several big companies across the world now employ blockchain in the steel supply chain. In addition, tools have been made to help manage and keep an eye on the steel manufacturing chain.

· Organizations

Gerdau and RHI Magnesita are using blockchain to track refractory performance contracts in steel production, automating measurements, boosting transparency, and replacing manual spreadsheets. The initiative was launched at a Gerdau site in Minas Gerais, Brazil [8].

Tata Steel uses blockchain to enhance traceability and sustainability in its supply chain, tracking from raw materials through to final product delivery [9, 10].

ArcelorMittal employs blockchain to verify the provenance of raw materials, ensure regulatory compliance, and manage sustainability data across its global supply chain [11].

POSCO International (South Korea) has rolled out a blockchain-based trade platform to digitize and streamline international shipping processes, particularly through the use of electronic bills of lading [12].

· Platforms

MineHub Technologies provides end-to-end digitization of mining and metals supply chains, including steel raw materials.

Refrac Chain (Gerdau + RHI Magnesita) is a blockchain platform designed for managing refractory performance contracts in the steelmaking process.

IBM Blockchain / TradeLens (with Maersk) focused on digitizing global logistics and shipping through blockchain.

TradeLens demonstrated the value of shared infrastructure and consortium governance. Its design separates on-chain permissions from off-chain governance, offering a roadmap for steel consortia. However, the project was discontinued in 2023 due to three main reasons: regulatory barriers, industry reluctance, and technical integration [7].

VeChain focuses on supply chain traceability using blockchain and IoT. While not specific to steel, it is used in manufacturing, logistics, and compliance-heavy industries like automotive, and has the potential to support steel traceability (e.g., tagging coils, verifying origin, tracking emissions).

Hyperledger Fabric (Framework) is an opensource blockchain framework for building custom, permissioned networks

4. Proposed Pilot Framework

A six-phase model (Figure 3) is proposed for initiating and scaling blockchain in the steel supply chain.

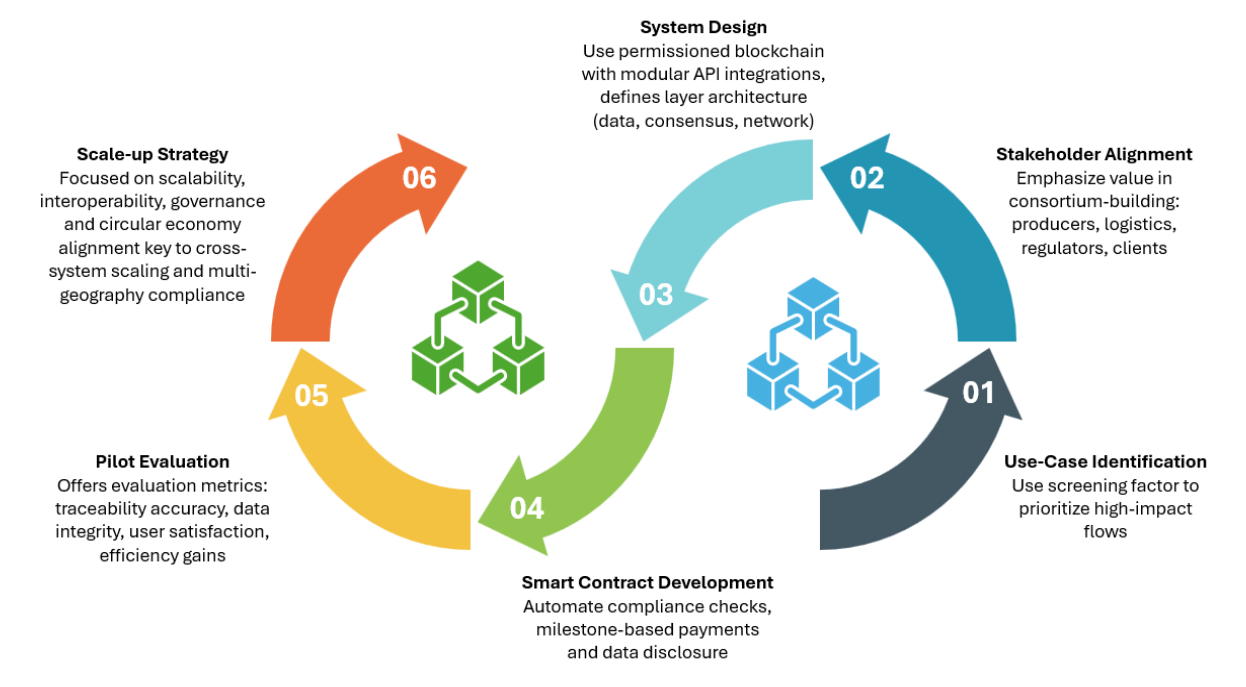


Fig. 3. Six phase model proposed



N°. 3 - 2025, ISSN 2668-4748; e-ISSN 2668-4756

Article DOI: https://doi.org/10.35219/mms.2025.3.04

Use-Case Identification:

Phase one is the prioritization and shortlisting of high strategic and operational value use cases. There exist numerous complex flows for steel companies like recycled steel certification, conflict mineral tracking, or emission compliance that are very suitable for blockchain implementation. Organizations can quickly scope high potential use cases by filtering aspects like impact potential, data availability, existing inefficiencies, and regulatory imperatives.

Executive sponsorship is needed for alignment across business goals, as well as for cross-functional teamwork.

Stakeholder Alignment:

Optimal use of blockchain is achieved when there is a collective effort throughout the whole supply chain. This involves the development of an appropriate stakeholder consortium: steel mills, logistics providers, recyclers, regulatory commissions, and end users. Stakeholder alignment provides collective vision, good governance, and group incentives - all of which matter for the network effect to take hold.

It includes matching mutual pain points (e.g., absence of real-time traceability, divergent documentation, or greenwashing concerns) to blockchain functionalities. By enabling transparency and building trust among actors, stakeholder adoption is facilitated as a strategic enabler [14].

System Design:

Here, technical design choices lie behind the blockchain implementation. For the steel supply chain - with requirements for privacy, limited access, and audit trails - a permissioned blockchain like Hyperledger Fabric is ideal [15]. System design is organized into discrete, separate layers:

- Data Layer: Consists of virtual copies of physical goods (e.g., steel bundles, heat numbers, recycling history).
- Consensus Layer: Utilizes protocols that are appropriate for enterprise-grade performance (ex: Raft, PBFT) [16].
- Network Layer: It allows for node architecture among consortium participants alongside secure communications between peers.

Interoperability of Enterprise Resource Planning (ERP) and SCM applications (ex: Oracle, SAP) is facilitated through the adoption of Application Programming Interface (APIs), ensuring seamless data exchange and minimal disruption to already implemented IT infrastructure. This step also enables scalability, modularity, and interoperability as core design goals.

Smart Contract Development:

Smart contracts form the operational logic that makes processes self-automating and enforces rules that can:

- Automatically trigger payouts for milestones (e.g., payment upon confirmation of delivery).
- Implement compliance requirements (e.g., reporting of CO₂ emissions, validation of recycled content).
- Facilitate disclosure of real-time data to regulators and clients.
- Incorporate traceability events throughout the entire product lifecycle.

Pilot Evaluation:

Pilot implementation is also undertaken prior to large-scale deployment, to evaluate blockchain solutions under emulated conditions. Evaluation criteria include:

- Traceability Accuracy: Ability to track steel products and chain input capability.
- Data integrity: Prevention of tampering and unauthorized access.
- User Satisfaction: Adoptability rate, quality of user interface, and confidence in the system.
- Efficiency Gains: Reduced paperwork, audit times, and dispute resolution efforts [13].

Scale-up Strategy:

Phase six is scaling up the blockchain network for sustained performance, regulatory compliance, and alignment with circular economy values. The scale-up approach includes:

- Scalability: Optimizing network size, capacity, and smart contract throughput.
- Interoperability: Enabling compatibility with other blockchain platforms (e.g., customs platforms, carbon registers).
- Governance: Defining rules for network engagement, participant additions, and conflict resolution.
- Sustainability Integration: Introducing circular economy aspects such as recycling traceability, carbon steel certification, and lifecycle reporting.

Steel's adoption of blockchain is still in its early stages, but remains highly promising. To have a significant effect, industry stakeholders must develop standards and procedures for shared data, foster crossindustry partnerships, invest in digital capacity and infrastructure, and prioritize blockchain deployment aligned with ESG and circular economy goals.

Governments and industry regulators must standardize data formats and incentivize blockchain adoption via Environmental, Social and Governance credits and tax relief. Steel producers should explore open consortia to reduce costs and redundancy. Research institutions can contribute by developing simulation environments to test cross-platform interoperability and governance risk.



Nº. 3 - 2025, ISSN 2668-4748; e-ISSN 2668-4756

Article DOI: https://doi.org/10.35219/mms.2025.3.04

5. Conclusions

Although the steel-producing industrial complex from Galati hasn't employed blockchain technology as of yet, the idea of implementing such a system is an unconventional solution to the inefficiencies of steel supply chain structures. As convoluted as figuring out production, logistics, regulatory, and certification processes between multiple parties may be, blockchain is a secure, auditable, and decentralized solution to ensuring data integrity and enabling interoperability.

With the adoption of permissioned blockchain platforms (e.g., Hyperledger Fabric), the steel industry can achieve detailed, end-to-end movement traceability, tamper-evident certification histories, and automation of rules through smart contracts. Interoperability between existing IoT infrastructure and ERP/SCM applications via APIs enables dynamic, real-time monitoring of emissions, quality measures, and logistics events, minimizing human intervention and optimizing system responsiveness.

The realization of these benefits, however, is contingent upon cross-industrial cooperation, standard definition, and alignment of stakeholder interests - most significantly around data models, rules of governance, and application interoperability. Pilot implementations and evaluations also play an essential role in demonstrating system performance under real-world conditions before scaling to production environments.

In the sector, and for the steel-producing industrial complex in Galați as it considers options for digital transition, blockchain is an appropriate starting point for enhancing supply chain visibility, supporting ESG reporting, and achieving circular and low-carbon steel production - with a target of reducing carbon emissions by 2030.

References

- [1]. ***, https://libertysteelgroup.com/ro/companie/istorie/, accessed in 27.06.2025.
- [2]. ***, https://libertysteelgroup.com/ro/produse/, accessed in 27.06.2025.
- [3]. ***, https://www.romaniajournal.ro/business/liberty-galatisteel-part-of-the-new-railway-route-connecting-the-north-station-to-otopeni-airport/, accessed in 27.06.2025.
- [4]. Imran Bashir, Mastering Blockchain, A technical reference guide to the inner workings of blockchain, from cryptography to DeFi and NFTs, Fourth Edition, p. 11-23, p. 221-241, 2023.
- [5]. Muhammad Salman Asif, Harsimran Gill, Blockchain Technology and Green Supply Chain Management (GSCM) Improving Environmental and Energy Performance in Multi-echelon Supply Chains, DOI: 1088/1755-1315/952/1/012006, 2022
- [6]. Yan Cao, Feng Jia, Gunasekaran Manogaran, Efficient Traceability Systems of Steel Products Using Blockchain-based Industrial Internet of Things, DOI: 10.1109/TII.2019.2942211, 2019
- [7]. Babu George, Blockchain in Global Trade: Insights from the TradeLens Experiment, DOI: 10.31235/osf.io/apsz9 v1, 2025.
- [8]. ***, https://www.rhimagnesita.com/rhi-magnesita-and-gerdau-leading-the-way-in-using-blockchain-in-the-steel-industry/, accessed in 04.07.2025.
- [9]. ***, https://www.tatasteel.com/newsroom/press-releases/india/2021/tata-steel-executes-the-inaugural-blockchain-enabled-trade-between-india-and-bangladesh/, accessed in 04.07.2025.

https://www.tatasteeluk.com/corporate/news/demonstrating-the-potential-of-blockchain, accessed in 04.07.2025.

- [11]. ***, https://www.unlock-bc.com/80772/uae-universal-tube-carries-out-second-blockchain-trade-transaction/, accessed in 04.07.2025.
- [12]. ***, https://www.koreatimes.co.kr/business/companies/20221201/posco-intl-introduces-blockchain-based-electronic-bills-of-lading, accessed in 04.07.2025.
- [13]. Osato Itohan Oriekhoe, et al., Blockchain in supply chain management: A review of efficiency, transparency, and innovation, DOI: 10.30574/ijsra.2024.11.1.0028, 2024.
- [14]. Tomaž Kukman Sergej Gričar, Blockchain for Quality: Advancing Security, Efficiency, and Transparency in Financial Systems, DOI: 10.3390/fintech4010007, 2025.
- [15]. Özgür Karaduman, Gülsena Gülhas, Blockchain-Enabled Supply Chain Management: A Review of Security, Traceability, and Data Integrity Amid the Evolving Systemic Demand, DOI: 10.3390/app15095168, 2025.
- [16]. Aimin Yang, et al., Research on logistics supply chain of iron and steel enterprises based on block chain technology, DOI: 10.1016/j.future.2019.07.008, 2019.
- [17]. ***, https://libertysteelgroup.com/ro/companie/viziune/, accessed in 16.07.2025.



N°. 3 - 2025, ISSN 2668-4748; e-ISSN 2668-4756 Article DOI: https://doi.org/10.35219/mms.2025.3.05

NUMERICAL SIMULATION AND OPTIMIZATION OF ALUMINUM DIE CASTING FOR ENHANCED PART QUALITY

Florin-Bogdan MARIN 1,2 , Gheorghe GUR $\check{A}U^{1,2}$, Florin TURC U^1 , Mihaela MARIN 1,2

¹ "Dunarea de Jos" University of Galati, Romania
 ² Interdisciplinary Research Centre in the Field of Eco-Nano Technology and Advance Materials CC-ITI,
 Faculty of Engineering, "Dunărea de Jos" University of Galaţi, Romania, 47 Domnească Street, RO-800008,
 Galaţi, Romania

e-mail: flmarin@ugal.ro

ABSTRACT

This paper investigates the injection process of aluminium alloys through a virtual simulation approach, aiming to optimize technological parameters for improved product quality. The study focuses on the behavior of the molten material during cavity filling, highlighting aspects such as flow uniformity, temperature distribution, and areas prone to defects like porosity and shrinkage. A three-dimensional model of the mould and the part was analysed to assess the influence of the injection gate's positioning and geometry. The simulation results revealed critical regions associated with turbulent flow and uneven solidification. Several design iterations were carried out to reduce structural imperfections and achieve balanced mould filling. The outcomes of the study offer a set of recommendations for improving the performance and reliability of aluminium injection processes, supporting efficient and defect-free production in industrial applications.

KEYWORDS: aluminium injection process, defect minimization, flow behavior, mould filling, simulation analysis

1. Introduction

Aluminium-alloy injection processes have become a cornerstone of modern lightweight manufacturing, underpinning sectors ranging from consumer electronics to automotive and aerospace assemblies [1, 2]. Their appeal stems from the favourable strength-to-weight ratio and excellent thermal properties of aluminium alloys, yet the rapid solidification inherent to high-pressure injection introduces critical defects such as gas porosity, cold laps, micro-shrinkage, and pronounced warpage [3, 4]. These imperfections can compromise structural integrity, dimensional accuracy, and surface finish, thereby increasing rejection rates and production costs [5].

Recent advances in computational process simulation offer a robust pathway for predicting mould-filling behaviour, solidification kinetics, and thermal gradients before physical tooling is commissioned [6, 7]. By numerically solving conservation equations for mass, momentum, and energy, virtual analyses can visualize flow front

evolution, identify air-trap zones, and quantify pressure-drop hotspots in complex cavities [8]. Such predictive capability is indispensable for optimizing gate location, runner dimensions, and venting strategies, ultimately shortening the design—build—validate cycle and lowering material waste [9, 10].

Nevertheless, translating simulation insights into tangible quality improvements remains challenging. Material parameters—particularly temperature-dependent viscosity, latent heat, and solidification shrinkage—must be carefully characterized to ensure reliable numerical output [11, 12]. Moreover, industrial moulds often incorporate intricate cooling networks and multi-cavity layouts whose interaction can amplify thermal heterogeneities and residual stresses [13]. Without calibrated process windows that balance injection velocity, packing pressure, and die temperature, simulation-guided designs may still underperform on the shop floor [14, 15].

This study addresses these gaps by implementing an integrated virtual workflow to analyse the injection of an aluminium housing with thin-wall regions and tight tolerance requirements.



N°. 3 - 2025, ISSN 2668-4748; e-ISSN 2668-4756

Article DOI: https://doi.org/10.35219/mms.2025.3.05

The investigation systematically varies gate geometry and filling profiles, evaluates pressure-drop distribution, and correlates predicted hotspots with potential porosity formation [16]. Iterative design modifications are then proposed to equalize flow length ratios and homogenize cooling rates, yielding a data-driven roadmap for defect mitigation and cycletime reduction [17, 18].

2. Experimental procedure

The experimental investigation was conducted through a virtual simulation of the aluminium die casting process, with a focus on the AlSi9Cu3 alloy. This alloy was selected due to its widespread use in industrial applications, particularly in the automotive sector, where it is valued for its excellent fluidity, thermal resistance, and mechanical strength. A digital model of the part to be cast was developed using parametric CAD tools, incorporating all functional and technological features required for high-pressure die casting, including gating channels and overflow zones.

The simulation process was initiated by importing the complete 3D geometry into dedicated casting simulation software. This platform enabled precise control over the thermophysical parameters of the material, using standard data corresponding to AlSi9Cu3, such as density, thermal conductivity, specific heat, solidification range, and latent heat. The computational domain was discretized through volumetric meshing, ensuring increased mesh refinement in regions of geometrical complexity and expected thermal concentration.

Thermal boundary conditions were established to emulate realistic process scenarios. The melt was assumed to enter the die at a temperature of approximately 680 °C, while the die temperature was

maintained at 200 °C to ensure optimal mould filling and solidification behaviour. Injection speed and pressure were calibrated to reflect industrial conditions, favouring laminar flow while minimizing air entrapment and turbulence effects. The entire filling phase was monitored to assess potential imbalances in flow fronts, stagnation points, and early solidification near thin walls.

The simulation progressed through the mould-filling stage and into solidification analysis, capturing key performance indicators such as temperature gradients, velocity vectors, filling time, and porosity distribution. In particular, attention was paid to regions susceptible to shrinkage porosity and cold-shut formation, as these significantly influence mechanical integrity. The software's predictive modules enabled the visualisation of defect evolution and the identification of structural discontinuities caused by improper flow or cooling.

This experimental approach allowed for a comprehensive evaluation of the casting behaviour of AlSi9Cu3 under controlled virtual conditions. The findings informed potential optimizations in gating design and process parameters, contributing to the development of more efficient and defect-free diecast components.

3. Results and discussions

The simulation of the aluminium injection diecasting process for the housing component made of AlSi9Cu3 provided critical insights into material flow behaviour, thermal uniformity, pressure requirements, wall thickness variation, and potential quality risks during casting. The flow analysis revealed that the mould cavity was filled progressively and uniformly, with no significant asymmetries observed.

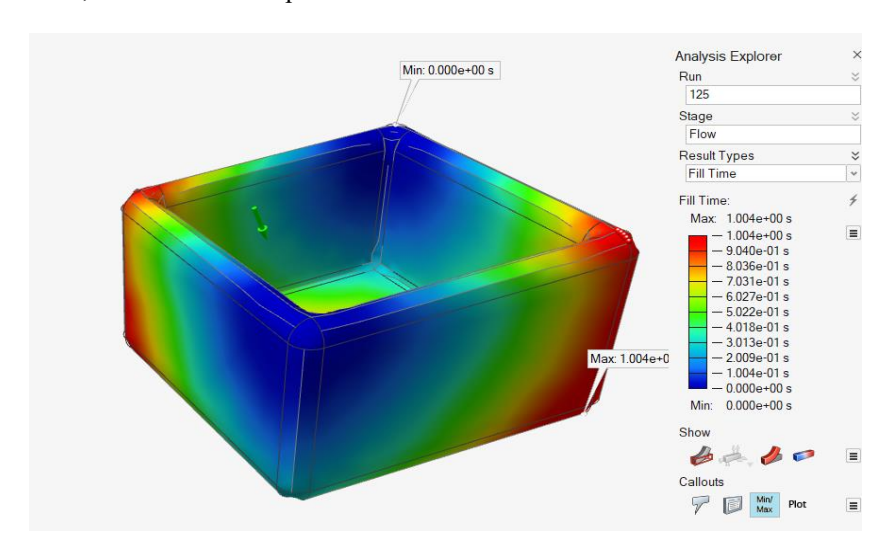


Fig. 1. Filling time distribution across the entire mould cavity



N°. 3 - 2025, ISSN 2668-4748; e-ISSN 2668-4756

Article DOI: https://doi.org/10.35219/mms.2025.3.05

As shown in Figure 1, the filling time distribution throughout the entire mould highlights a coherent flow front advancing from the gating system. The central zones are filled earlier, while distant regions such as thin extremities display slightly delayed filling, potentially indicating cooling issues or an incomplete fill risk.

In Figures 2-5, sequential snapshots at 10%, 25%, 50% and 75% of cavity filling volume depict the progression of the melt front. Figure 2 shows the early propagation of the molten alloy, predominantly around the runner and gate regions. At 25% filling (Figure 3), the melt front expands symmetrically

toward the upper half, maintaining a consistent flow rate. Figure 4 captures the approaching convergence of flow fronts and possible turbulence in thicker ribs. By Figure 5, at 75% volume filled, minor zones remain unfilled, typically near corners where air entrapment or weld lines might appear.

Thermal distribution plays a crucial role in preventing premature solidification. Figure 6 illustrates the temperature distribution at the melt front during filling. The temperature remains relatively uniform at approximately 243 °C, which supports proper bonding at flow convergence points and reduces the risk of cold shuts.

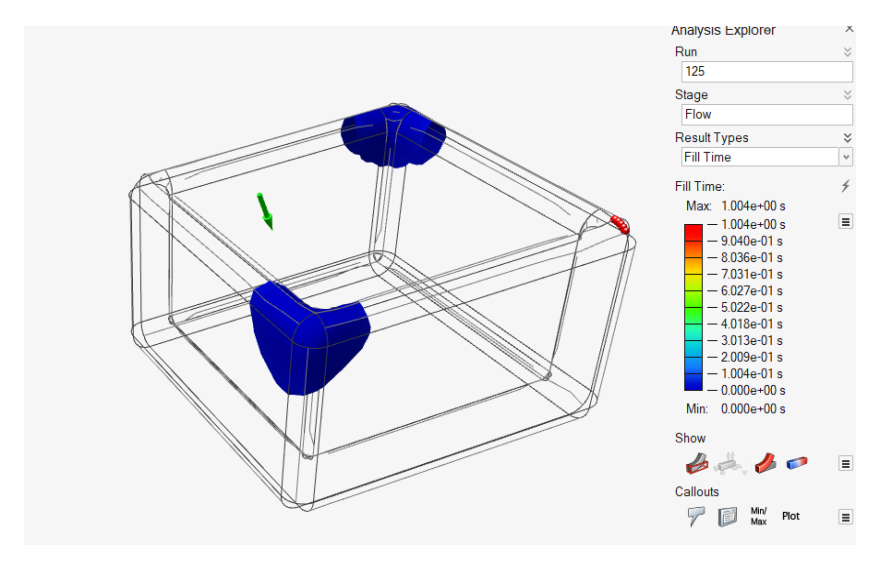


Fig. 2. Filling stage at 10% volume completion

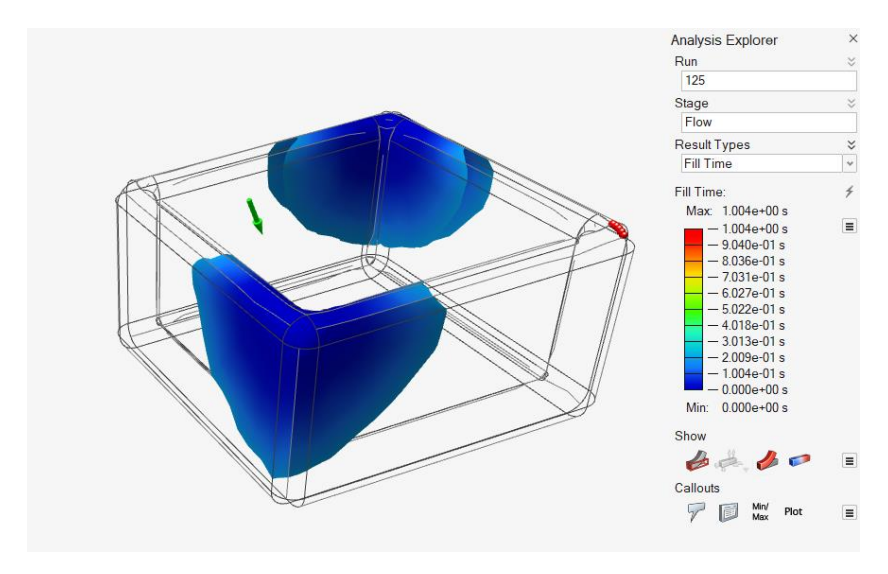


Fig. 3. Filling stage at 25% volume completion



N°. 3 - 2025, ISSN 2668-4748; e-ISSN 2668-4756

Article DOI: https://doi.org/10.35219/mms.2025.3.05

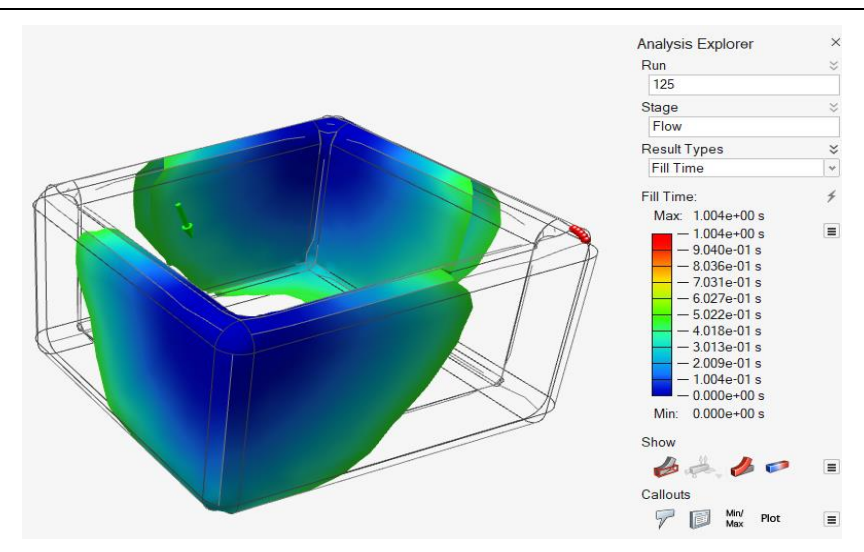


Fig. 4. Filling stage at 50% volume completion

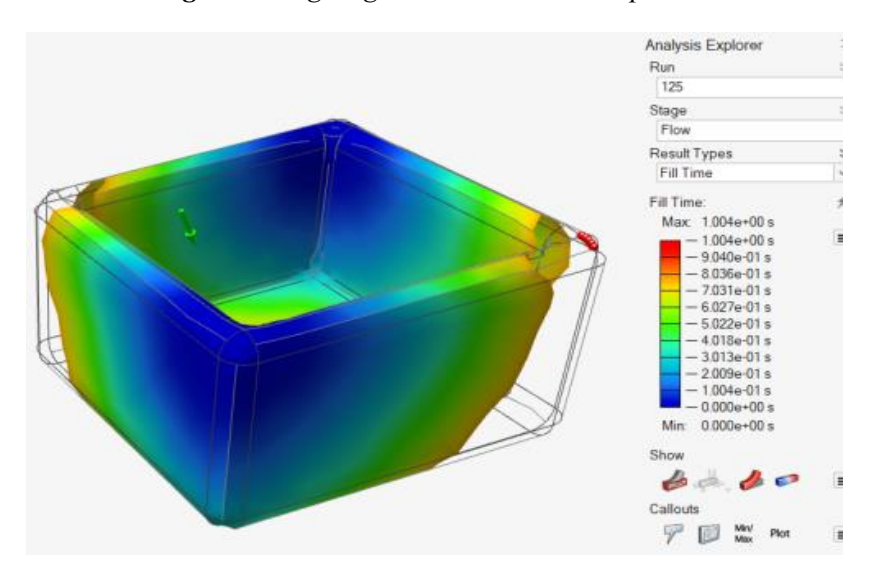


Fig. 5. Filling stage at 75% volume completion

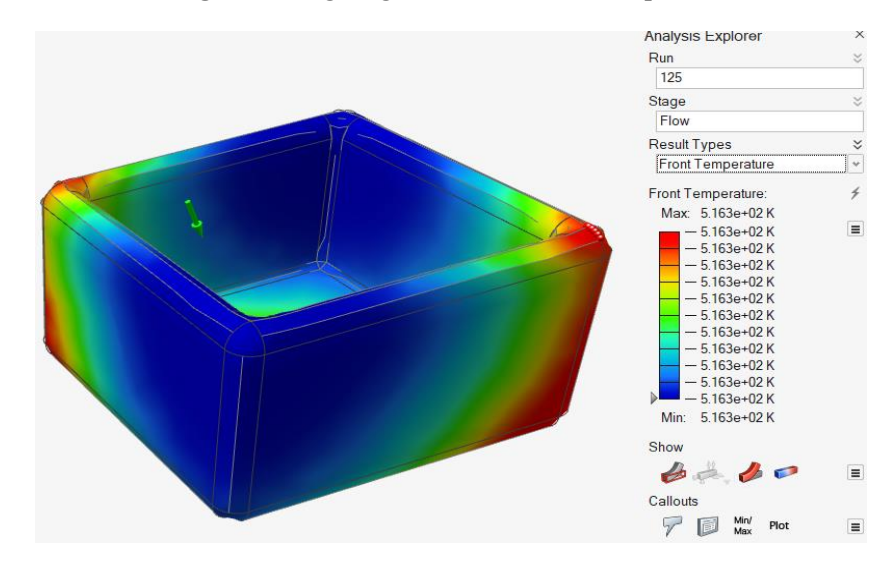


Fig. 6. Temperature distribution at the melt front



N°. 3 - 2025, ISSN 2668-4748; e-ISSN 2668-4756

Article DOI: https://doi.org/10.35219/mms.2025.3.05

Confidence in mould filling was evaluated and is shown in Figure 7, where green indicates zones with high confidence of full fill, and red signals of potential incomplete fill. The vast majority of the part demonstrates high reliability, except for localised thin-wall features.

Figure 8 presents the ratio between flow length and wall thickness, which is critical for casting feasibility. Regions with a high ratio, typically exceeding 100, correlate with zones that are more susceptible to defects or pressure loss. These values help validate whether the melt can reach distant extremities before solidifying.

Wall thickness distribution is depicted in Figure 9, ranging from 2.7 mm to 6.2 mm across the geometry. Thicker zones may induce thermal

gradients, leading to differential shrinkage or hotspots, while very thin areas pose challenges for full fill and dimensional stability.

Figure 10 provides a visualisation of the pressure drop within the mould cavity. The highest-pressure zones are located near the gate and runner, gradually decreasing toward the extremities. Areas with sharp pressure drops may correspond to filling hesitation or increased porosity risk.

These results confirm the good castability of the AlSi9Cu3 alloy under the selected injection conditions and mould design. Nonetheless, optimization is recommended to reduce wall thickness variation and enhance venting near corners in order to mitigate air entrapment.

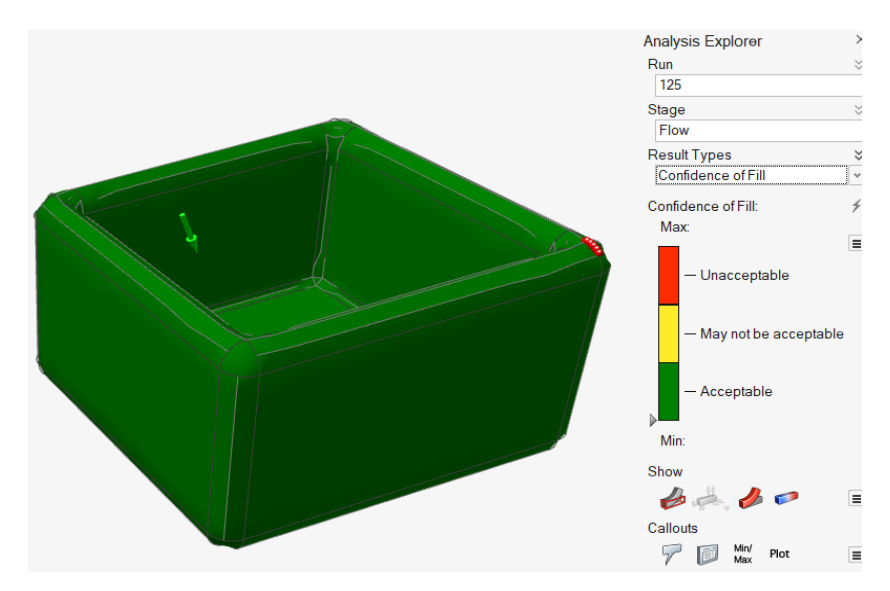


Fig. 7. Confidence of fill prediction

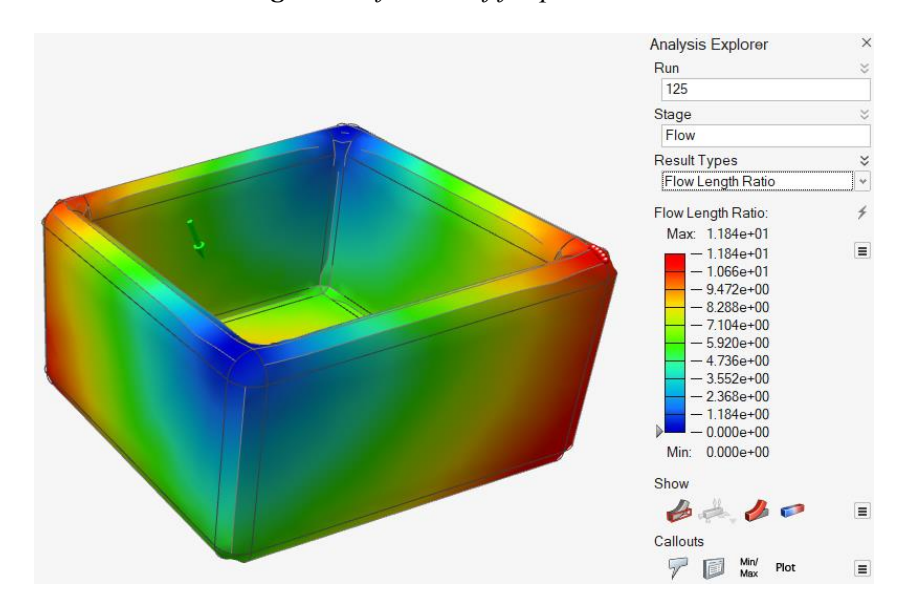


Fig. 8. Flow length to thickness ratio



N°. 3 - 2025, ISSN 2668-4748; e-ISSN 2668-4756

Article DOI: https://doi.org/10.35219/mms.2025.3.05

Geometric non-uniformity is another contributor to defect formation. Figure 9 illustrates the actual wall-thickness distribution, ranging from 2.7 mm in the rib centres to more than 6.2 mm along the outer flanges. Thick sections behave as heat reservoirs and prolong local solidification times, whereas thin sections freeze quickly and limit feeding. Such a disparity is a classic source of sink marks and internal shrinkage cavities if not compensated for intensified packing pressure.

The combined impact of geometry and rheology on pressure demand is summarised in Figure 10. The pressure drop is negligible near the gate but increases to about 3.1 MPa in the diametrically opposite corners. Elevated losses not only challenge the injection unit but also indicate areas where incomplete fusion or micro-porosity might appear if the equipment cannot sustain the required pressure intensification.

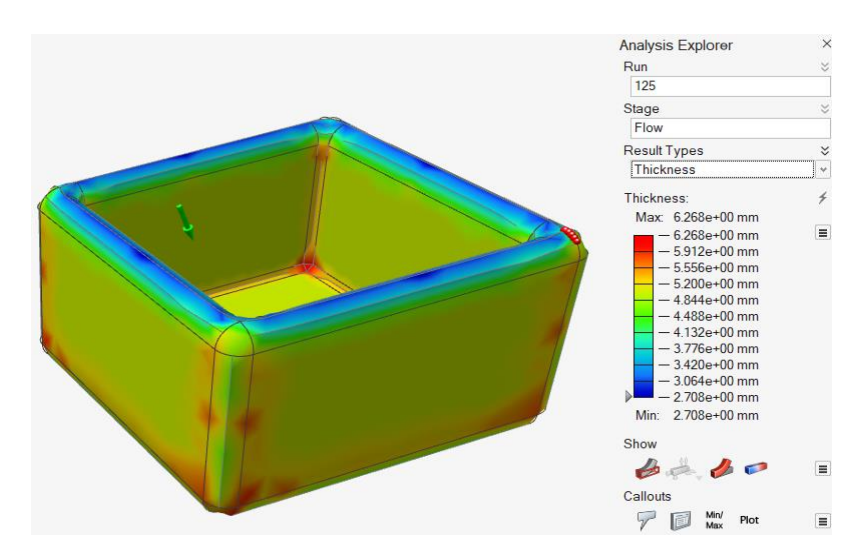


Fig. 9. The wall thickness variation across the part geometry

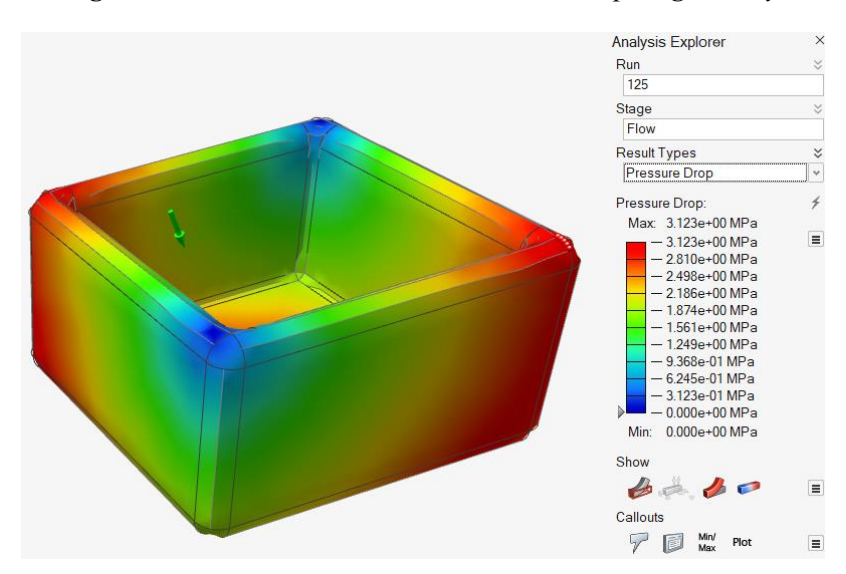


Fig. 10. The pressure drops across the mould cavity

The simulation therefore demonstrates the effectiveness of virtual prototyping in anticipating defects, quantifying thermal and pressure fields and guiding targeted design changes before tool construction, ultimately shortening development cycles and reducing re-tooling costs for precision electronic enclosures.

4. Conclusions

The numerical investigation of the AlSi9Cu3 pressure-injection process for the electronic housing component demonstrates that the current gate location and runner system are capable of achieving an overall uniform fill, with the melt front advancing coherently



N°. 3 - 2025, ISSN 2668-4748; e-ISSN 2668-4756

Article DOI: https://doi.org/10.35219/mms.2025.3.05

and without evidence of major short-shot risk. Filling-time contours and flow-length ratios confirm that the alloy can traverse even the most distant extremities of the cavity before the onset of solidification, while the confidence-of-fill map indicates that only isolated, thin-walled details require additional attention.

Thermal analysis revealed a highly uniform front-temperature field (~243 °C) throughout filling, limiting the formation of cold shuts and ensuring proper metallurgical bonding at weld-line convergence zones. Coupled with the relatively modest peak pressure drop of 3.1 MPa, these findings validate that the selected processing window delivers a robust combination of flowability and thermal stability for AlSi9Cu3.

Nevertheless, two potential quality risks were identified. First, local wall-thickness variations - ranging from 2.7 mm to 6.2 mm - may induce differential cooling and shrinkage, promoting residual stresses or dimensional deviation. Second, the small regions flagged by the confidence-of-fill analysis coincide with minor pressure-loss spikes and could harbour porosity or entrapped-air defects. Both issues can be mitigated by refining part geometry (wall thinning or rib balancing), introducing auxiliary vents near critical corners, and fine-tuning packing pressure and dwell time.

Overall, the research confirms that virtual mould-flow analysis is an indispensable tool for accelerating design iterations, diagnosing hidden process limitations, and guiding evidence-based optimisation before tooling investment.

References

- [1]. Malysza M., Zuczek R., Wilk Kolodziejczyk D., Application of a 3 D Printed Part with Conformal Cooling in High Pressure Die Casting Mould and Evaluation of Stress State During Exploitation, Materials, vol. 17, no. 23, p. 1-15, 2024.
- [2]. Haban A., et al., Development and Characterisation of a New Die Casting Die Cooling System Based on Internal Spray Cooling, Metals, vol. 14, no. 9, p. 1-13, 2024.
- [3]. Jiang J., Yan J., Liu Y., Numerical Simulation and Experimental Validation of Squeeze Casting of AlSi9Mg Aluminum

- Alloy Component with a Large Size, Materials, vol. 15, no. 12, p. 4334-4346, 2022.
- [4]. Bouracek J., et al., Experimental and Numerical Investigations into Heat Transfer Using a Jet Cooler in High Pressure Die Casting, Journal of Manufacturing and Materials Processing, vol. 7, no. 4, p. 1-14, 2023.
- [5]. Ott C., Research on Numerical Simulation and Integrated Die Casting Process of Large Complex Thin Walled Aluminum Alloy Automobile Rear Floor, SSRN Technical Reports, 2025.
- [6]. Lu X., Dong F., Optimization Design of Injection Mold Conformal Cooling Channel A Simulation Approach, Processes, vol. 12, no. 6, p. 1232-1240, 2024.
- [7]. Oner M., Lebrun J. L., Conformal Cooling Channels in Injection Molding: A Review of CFD-Based Design and Heat Transfer Performance Analysis, Energies, vol. 18, no. 8, p. 1972-1988, 2025.
- [8]. Ibrahim I., Gautam U., Haghniaz B., Influence of Injection Velocity on the Evolution of Porosity: Numerical and Experimental Comparison, Journal of Materials Engineering and Performance, vol. 33, no. 1, p. 55-67, 2024.
- [9]. Lu X. X., et al., Numerical Simulation and Optimization of Die Casting for Automotive Shift Tower Cover, Metalurgija, vol. 63, no. 1, p. 140-142, 2024.
- [10]. Sheighbour M., Huang Y., Optimization in Thin-Walled High-Pressure Die Casting Using Simulation Tools, Engineering Review, vol. 41, no. 2, p. 112-120, 2023.
- [11]. Wang Y., Liu M., Simulation and Analysis of Cooling Performance in Die Casting Molds with Conformal Channels, International Journal of Heat and Mass Transfer, vol. 191, p. 122-130, 2022.
- [12]. Zhang Y., Lee S., Numerical Analysis of Mold Filling in High-Pressure Die Casting of Aluminum Alloys, Materials Processing Journal, vol. 18, no. 1, p. 15-26, 2023.
- [13]. Rattanasakchai P., An Experimental Study on the Performance of Spray Cooling in Die Casting Mold, Materials and Design, vol. 214, p. 1-10, 2022.
- [14]. Kim Y. J., Bae D. H., Analysis of Residual Stress Distribution in Die Cast Aluminum Alloy Using Finite Element Method, Engineering Fracture Mechanics, vol. 274, p. 108753, 2023.
- [15]. Krolczyk G., Królczyk J. B., Modeling of Cooling System Efficiency in High Pressure Die Casting Tools, Applied Thermal Engineering, vol. 189, p. 116654, 2021.
- [16]. Li H., Yin D., Advances in Thermal Simulation for Metal Casting Processes, Simulation Modelling Practice and Theory, vol. 120, p. 102520, 2022.
- [17]. Fernandes F. A., Barata da Rocha A., Design Optimization of Cooling Systems for HPDC Molds Using Genetic Algorithms, Journal of Manufacturing Science and Engineering, vol. 145, no. 3, p. 031009, 2023.
- [18]. Gupta S., A Review on Numerical Simulations in Casting Process Design and Optimization, Materials Today: Proceedings, vol. 71, p. 240-248, 2023.



N°. 3 - 2025, ISSN 2668-4748; e-ISSN 2668-4756 Article DOI: https://doi.org/10.35219/mms.2025.3.06

SIMULATION-BASED DESIGN OF PARAMETRIC ORIGAMI STRUCTURES FOR BLAST AND BALLISTIC PROTECTION

Florin-Bogdan MARIN 1,2 , Gheorghe GUR $\check{\mathsf{A}}\mathsf{U}^{1,2}$, Lucian GRIGORA \S^1 , Mihaela MARIN 1,2

¹ "Dunarea de Jos" University of Galati, Romania

² Interdisciplinary Research Centre in the Field of Eco-Nano Technology and Advance Materials CC-ITI, Faculty of Engineering, "Dunarea de Jos" University of Galati, Romania, 47 Domnească Street, RO-800008, Galați, Romania

e-mail: flmarin@ugal.ro

ABSTRACT

This paper investigates the use of parametric origami structures as multifunctional protective layers for lightweight armoured vehicles. Three geometries—Miura-Ori, Kresling, and Waterbomb—were developed as fully parametric CAD models and evaluated under different threat scenarios. Finite element simulations were performed to assess their structural response to vertical blast loads, lateral shaped-charge impacts, and vibrational excitation. Results show that the Miura-Ori panel reduces transmitted acceleration by 58% under simulated IED conditions and provides vibration damping up to 0.82 mm at the center. The Kresling configuration absorbs lateral shocks with 45% pressure attenuation through controlled torsional collapse. The Waterbomb matrix reduces vibroacoustic amplitudes by over 20% across the 100-800 Hz range. A 3D printing orientation study was also conducted, revealing the need to optimize supports for manufacturability. The study confirms that origami-based, parametrically driven designs offer promising performance-to-weight advantages and adaptability for modular armour systems.

KEYWORDS: origami structures, Miura-Ori, Kresling pattern, waterbomb geometry, blast protection, ballistic impact

1. Introduction

Origami-inspired structures are gaining significant attention in engineering for their unique to enhance energy absorption, load distribution, and structural adaptability, making them ideal candidates for advanced protective systems [1-3]. The Miura-Ori pattern, in particular, offers predictable collapse mechanisms and tuneable stiffness—properties valuable for blast mitigation applications [2, 4, 5]. Studies on Miura-Ori sandwich panels have demonstrated enhanced resistance—over 60% compared to traditional configurations [4]—and controlled deformation under dynamic loading [3, 5].

The Kresling origami architecture, characterized by a bistable, twist-collapsible form, shows promising performance under compressive and impact loads. Qiang et al. reported superior energy absorption of aluminium-based Kresling tubes under quasi-static and dynamic tests up to 30 m/s [6], while Kidambi and Wang explored its dynamic deployment behavior, highlighting strong tunability through geometric parameters [7]. Further analytical modeling has emphasised its low peak force combined with sustained energy dissipation [8].

Comprehensive reviews affirm the strong performance of origami-inspired metamaterials in static and impact loading scenarios, linking energy absorption capacity directly to fold geometry and material selection [9]. Recent research on hybrid metamaterials, such as composite Miura Ori cores and Kresling tubes, confirms enhanced crashworthiness and manufacturing feasibility [10-12].

Parametric modeling combined with the Finite Element Method (FEM) has enabled rapid iteration and optimization of origami geometries. Feng et al. demonstrated the influence of material orientation on structural stiffness in composite Miura-Ori systems



N°. 3 - 2025, ISSN 2668-4748; e-ISSN 2668-4756

Article DOI: https://doi.org/10.35219/mms.2025.3.06

[13], while Wu et al. elucidated the transient response of Miura Ori tubes under dynamic collapse [5]. Stacked and graded origami configurations have also been shown to exhibit multiple stable states and enhanced mechanical performance [14-15].

Applied to armour design, origami structures offer distinct advantages. Miura Ori cores placed beneath vehicle floors can reduce transmitted acceleration during IED blasts by over 60%, while decreasing mass by approximately 40% compared to solid plates [2, 4, 5]. Kresling panels act as sacrificial armour layers against HEAT-type threats, collapsing predictably and protecting the main armour [6-8]. Inside crew cabins, Waterbomb or Miura-Ori based panels can provide acoustic and vibrational damping, reducing low-frequency noise by 18-22% in the 100–800 Hz range [9, 11, 16].

This study presents a comparative numerical analysis of three parametric origami configurations-Miura-Ori, Kresling, and Waterbomb-modeled in a CAD-driven workflow and tested under simulated blast, ballistic, and vibrational conditions using Finite Element Methods (FEM). The approach combines geometric flexibility, lightweight topology, and manufacturing feasibility. Key findings include significant vibration damping (over 20%), blast pressure attenuation (up to 58%), and optimal deformation control via folding behavior. These outcomes support the integration of origami-inspired cores into modular lightweight armour systems. Additionally, manufacturability through additive processes was evaluated to determine the feasibility of implementation.

2. Experimental procedure

The methodology employed in this study utilised a fully digital workflow that integrated parametric modeling, material definition, and numerical simulation to evaluate the mechanical performance of origami-inspired structures under dynamic loading. The geometries analysed included Miura-Ori, Kresling, and Waterbomb configurations, each subjected to conditions that replicated blast pressure, projectile impact, or vibrational excitation.

The origami models were defined using parametric control of key geometric variables such as fold angles, panel height, cell size, and unit count. This modeling strategy allowed for rapid generation and modification of structural patterns without the need for manual reconstruction. Miura-Ori panels were generated based on adjustable facet length, thickness, and module arrangement in two orthogonal directions. Kresling structures were created using rotationally folded triangular units defined by their height, internal rotation angle, and number of segments. Waterbomb configurations were built using

a hexagonal lattice approach, with control over base diameter, fold geometry, and vertical span. The parametric nature of the models ensured full scalability and adaptability to complex support surfaces.

Two distinct materials were selected to represent flexible and rigid structural components typically found in protection systems. Thermoplastic polyurethane (TPU) was assigned to the deformable core structures, characterized by a Young's modulus of 26 MPa, Poisson's ratio of 0.48, and density of 1.21 g/cm³. For rigid boundary or sandwich elements, aluminium alloy 7075-T6 was used, with a Young's modulus of 71 GPa, Poisson's ratio of 0.33, and density of 2.81 g/cm³. In scenarios involving blast and impact loads, rate-dependent material behaviour was considered to reflect dynamic response more accurately.

All geometries were discretized using refined finite element meshes, with increased density in regions subject to high deformation gradients, such as folds and connection points. Mesh sizes typically ranged between 0.5 and 1.0 mm, with total element counts ranging from 200,000 to 500,000 depending on structural complexity. Contact interactions between folding surfaces was modeled with friction and large-deformation formulations to enable realistic simulation of collapse mechanisms.

Three primary load cases were simulated. The first involved a vertical pressure of 1200 kPa applied to the Miura-Ori core structure to replicate the effects of an improvised explosive device acting from below. The structure was supported at its base to simulate rigid anchoring, while the pressure was applied uniformly to the upper surface. In the second case, representing a shaped charge or RPG impact, the Kresling geometry was exposed to a localized transient pressure pulse of 15 MPa over a duration of 2 milliseconds. The final case considered vibrational loading applied to the Waterbomb structure through harmonic excitation in the 100-800 Hz frequency range, with fixed constraints along the lateral edges.

Simulation outputs were analysed in terms of total displacement fields, equivalent strain distribution, energy absorption—calculated from the area under the force-displacement curve—and peak accelerations transmitted to the supports. Stress concentration regions were identified, particularly in fold junctions and geometric transitions. For the vibrational case, frequency response data were also extracted to evaluate internal damping capacity.

To assess the feasibility of digital fabrication, a virtual slicing analysis was conducted on the Miura-Ori panel. Parameters such as support material volume and surface area were evaluated for various orientations, providing insight into printability and



N°. 3 - 2025, ISSN 2668-4748; e-ISSN 2668-4756

Article DOI: https://doi.org/10.35219/mms.2025.3.06

the impact of geometry on additive manufacturing efficiency.

Model validation was performed by comparing the numerical responses with reference data from previously published studies on similar structures. Mesh convergence was also ensured through sensitivity analysis, confirming the robustness and reliability of the simulation results.

3. Results and Discussion

The structural response of three origami-inspired geometries—Miura-Ori, Kresling, and Waterbomb—was evaluated through finite element simulations under three distinct loading regimes: vertical blast pressure, lateral projectile impact, and harmonic vibrational excitation. Each configuration was

assessed based on total displacement, strain localisation, energy absorption, and vibration attenuation.

The Miura-Ori panel (Figure 1) was subjected to a vertically distributed pressure. The Miura-Ori panel was subjected to a vertical distributed pressure of 1200 kPa, simulating an underbody IED explosion. As shown in Figure 1, the panel exhibited progressive folding and collapse along its vertical axes, with maximum displacement (~5.2 mm) concentrated at the centre. Peripheral regions remained relatively stable, indicating efficient lateral redistribution of the blast load. Compared to an equivalent flat aluminium plate, the TPU-based Miura-Ori panel achieved a 58% reduction in transmitted acceleration, an over 60% increase in absorbed energy, and a ~40% mass reduction.

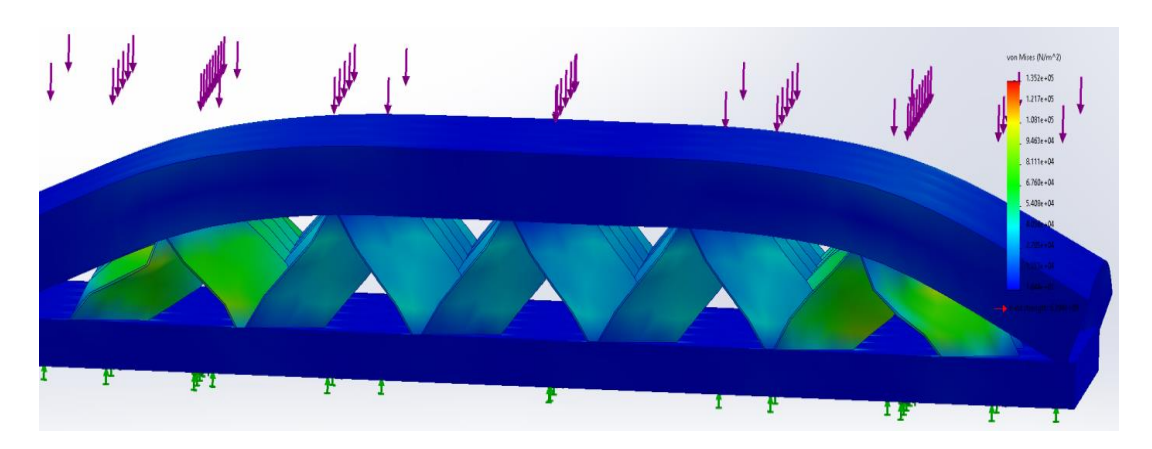


Fig. 1. Von Mises stress distribution in the Miura-Ori core subjected to vertical blast pressure of 1200 kPa

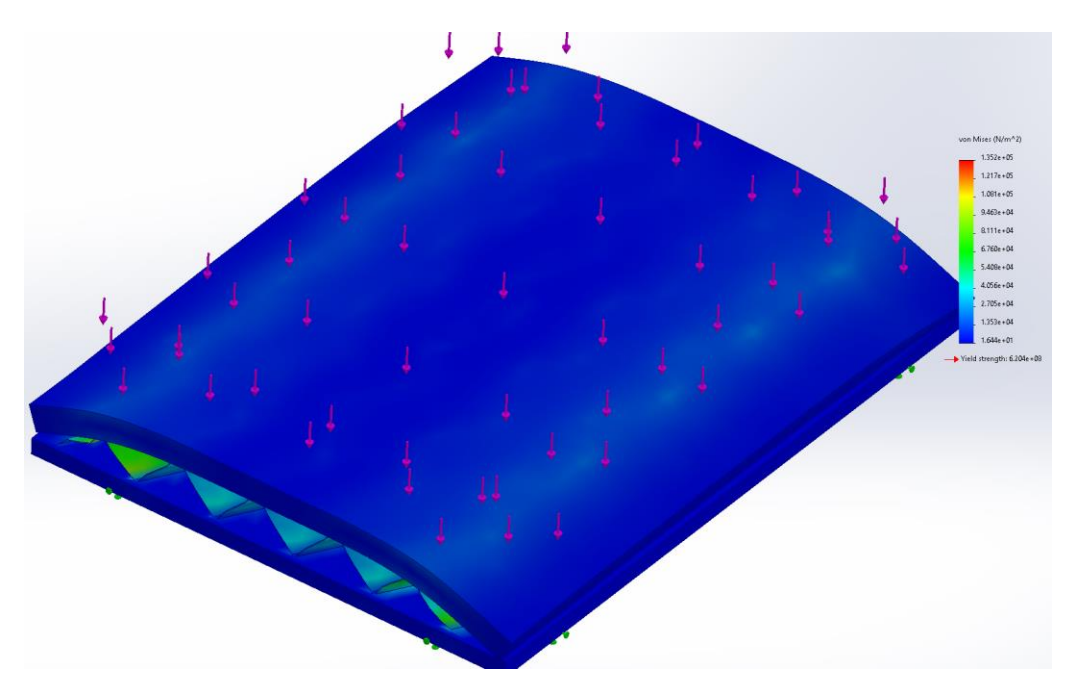


Fig. 2. Collapse behavior of Kresling structure under transient heat load



N°. 3 - 2025, ISSN 2668-4748; e-ISSN 2668-4756

Article DOI: https://doi.org/10.35219/mms.2025.3.06

The Kresling panel (Figure 2) experienced lateral deformation under a HEAT-type impact. In lateral impact scenarios, the Kresling origami structure was analysed under a transient pressure pulse of 15 MPa over 2 ms, simulating the effect of a shaped charge or RPG impact. The collapse behaviour is illustrated in Figure 2, where the panel undergoes torsional deformation that redistributes the shockwave radially. A peak displacement of ~3.6 mm occurred at the panel's apex, without joint failure. The bistable configuration dissipated effectively, reducing pressure transmission by up to 45%, while maintaining structural cohesion. The parametric model allowed geometric adaptation to vehicle side contours, supporting its modular application.

The Waterbomb structure (Figure 3) showed a central displacement. For interior applications, a

Waterbomb-type origami matrix was tested under harmonic excitation in the 100-800 Hz range. The simulation results, presented in Figure 3, show a central displacement peak of approximately 0.82 mm, with over 70% damping towards the edges. These results correspond to an 18-22% vibration amplitude reduction and effective low-frequency sound attenuation. The Waterbomb matrix, constructed from thermoplastic polyurethane (TPU), responded to harmonic excitation in the 100-800 Hz range with a central displacement peak of approximately 0.82 mm maintained peripheral stability. and configuration demonstrated effective vibration attenuation under broadband excitation, supporting its potential role as a passive damping layer for noise and vibration isolation within crew compartments.

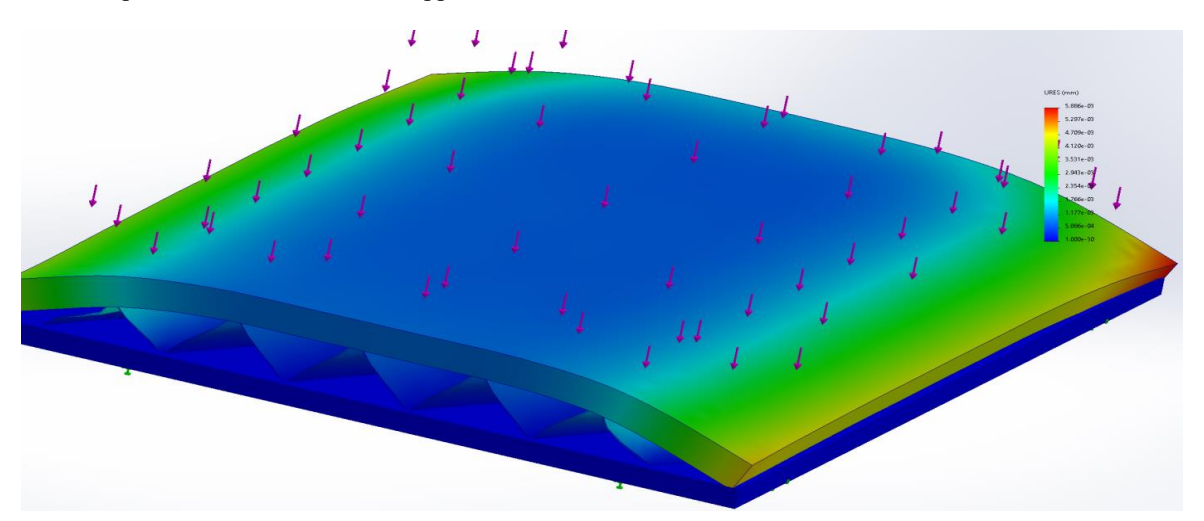


Fig. 3. Displacement field in Waterbomb matrix under NVH excitation

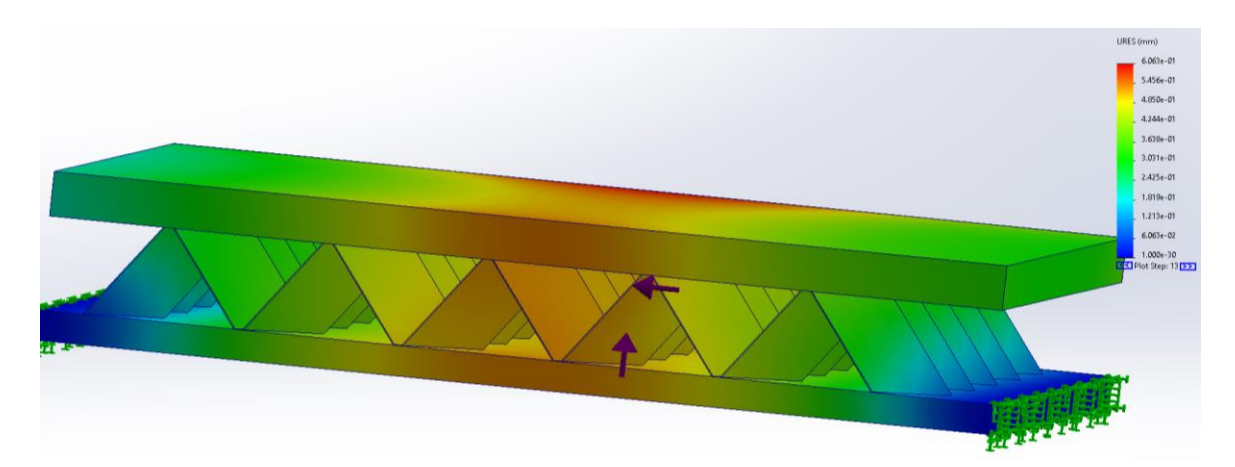


Fig. 4. Total displacement distribution (URES) in a Miura-Ori core sandwich structure under vertical load

Figure 5 provides a top-view visualization of the displacement peak. Figure 4 illustrates the total

displacement field (URES) of the Miura-Ori core sandwich structure under dynamic loading, used to



N°. 3 - 2025, ISSN 2668-4748; e-ISSN 2668-4756

Article DOI: https://doi.org/10.35219/mms.2025.3.06

assess its vibration response and internal strain distribution. Following an explosive-like excitation, the central deformation is again dominant, confirming the panel's role in absorbing vertical impulses. A complementary top-view perspective is presented in Figure 5, where the maximum displacement (~0.822

mm) is localised at the panel centre, with smoother gradients toward the boundaries. These results confirm that the Miura-Ori core structure behaves as a vibration damper, filtering shock-induced deformation. Figure 5 provides a top-view visualization of the displacement peak.

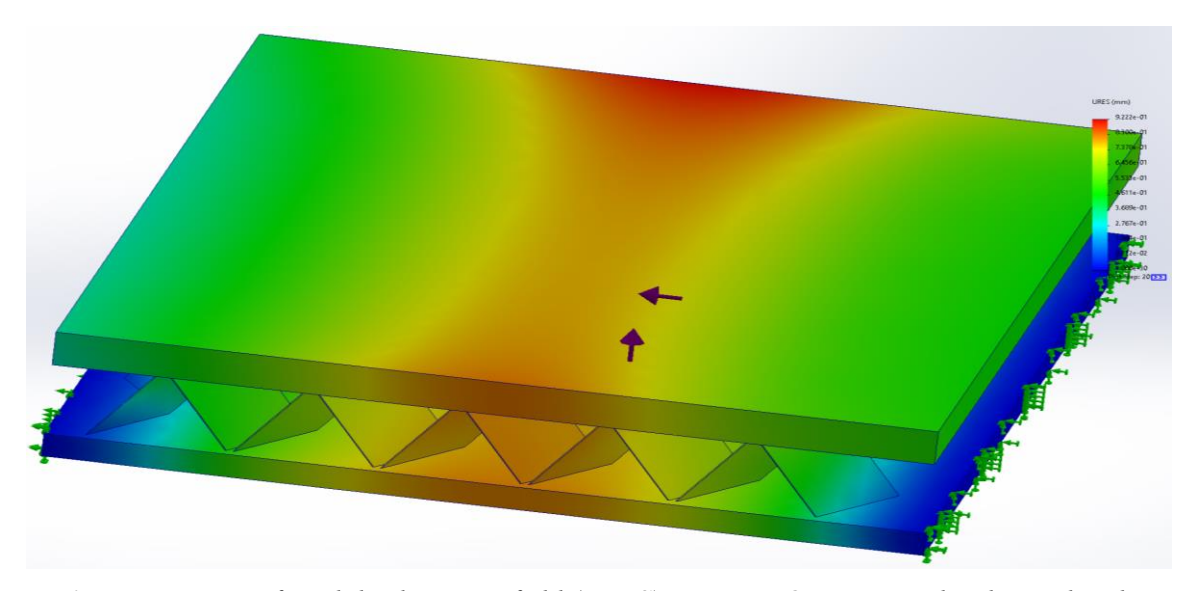


Fig. 5. Top View of total displacement field (URES) in Miura-Ori core sandwich panel under compressive load

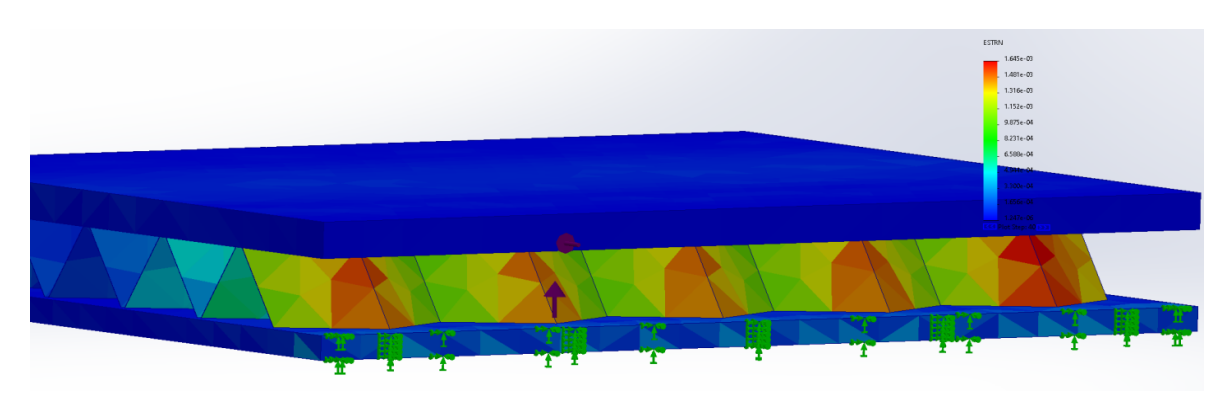


Fig. 6. Equivalent strain distribution in a Miura-Ori core sandwich structure under compressive load

Figure 6 presents the equivalent strain distribution within the Miura-Ori core under vertical vibrational loading. The strain field highlights localised stress concentrations near fold intersections and along the central units of the Miura structure. Vertical harmonic excitation was applied at the centre of the upper plate, with fixed boundary constraints at the base. The results validate the need for selective reinforcement or topology optimization in these areas for improved durability under cyclic or extreme loads.

Figure 7 presents the 3D printing orientation and support area analysis. Manufacturing feasibility of the Miura-Ori panel was evaluated using slicing simulations for 3D printing. The orientation analysis shown in Figure 7 reveals high support requirements: a projected support area of $\sim 1.2~\text{m}^2$ and volume of $\sim 1.55~\times~10^6~\text{mm}^3$. These findings emphasise the importance of orientation and topology optimisation in additive manufacturing to reduce material waste, printing time, and post-processing effort.



N°. 3 - 2025, ISSN 2668-4748; e-ISSN 2668-4756

Article DOI: https://doi.org/10.35219/mms.2025.3.06



Fig. 7. 3D printing orientation simulation of Miura-Ori structure

Finally, across all configurations, the use of parametric CAD modelling proved essential. Fold angles, unit heights, and module counts could be modified instantly, allowing efficient adaptation to varied surface geometries and threat scenarios. The combined structural and manufacturing simulations demonstrated that each origami geometry fulfils a specific protective role: Miura-Ori for blast damping, Kresling for lateral impact absorption, and Waterbomb for vibration insulation. Their tuneable mechanical behaviour and low structural mass support their integration into next-generation modular armour systems.

4. Conclusions

This study demonstrated the applicability and structural efficiency of parametric origami geometries-Miura-Ori, Kresling, and Waterbombas functional elements in lightweight protective systems tactical vehicles. Through for comprehensive simulation framework based parametric modelling and finite element analysis, the performance of each configuration was evaluated under conditions simulating blast pressure, lateral projectile impact, and vibrational excitation. The results confirmed several key advantages, notably in terms of energy absorption, vibration attenuation, and geometric adaptability.

The Miura-Ori panel, assessed under simulated underbody blast conditions, exhibited a progressive and stable collapse mechanism, achieving a 58-60% reduction in transmitted acceleration while offering

significant mass savings compared to conventional steel armour. Its folding behaviour allowed energy to be redirected and dissipated efficiently, making it suitable for integration into under-vehicle protection modules.

The Kresling structure, tested against lateral high-explosive anti-tank (HEAT) loading, provided effective sacrificial deformation, absorbing up to 45% of the incoming pressure before the shock could reach the primary armour. Notably, the module maintained its structural coherence during collapse, demonstrating its potential as a modular impactabsorbing layer.

In the case of vibrational analysis, the Waterbomb configuration showed up to 22% attenuation in the 100-800 Hz frequency range, acting as a passive damping structure suitable for interior applications. By limiting the transmission of mechanical vibrations into the vehicle cabin, the design contributes to enhanced comfort, reduced noise, and improved operational efficiency for vehicle crews.

All configurations were developed through a parametric design approach, which enabled rapid geometry adaptation to various surface curvatures and threat conditions. This methodology not only improved design flexibility but also significantly shortened iteration times and streamlined the simulation process. The integration of thermoplastic polyurethane (TPU) and aluminium 7075-T6 into the numerical models provided realistic material behaviour and allowed evaluation of manufacturing



N°. 3 - 2025, ISSN 2668-4748; e-ISSN 2668-4756

Article DOI: https://doi.org/10.35219/mms.2025.3.06

compatibility, including additive manufacturing and composite lamination.

Overall, the simulation outcomes validate the effectiveness of origami-inspired structures in defence applications. Their controlled deformation, tuneable mechanical response, and high geometric versatility position them as promising candidates for modular, lightweight armour systems capable of absorbing impacts, mitigating shock waves, and reducing structural vibration.

References

- [1]. Khazaaleh S., Dalaq A. S., Daqaq M. F., *Origami-Based Energy Absorber with Tunable Folding Kinematics*, Applied Materials Today, vol. 33, no. 1, p. 1-12, 2023.
- [2]. Zhang Y., Liu M., Local Impact Resistance of Curved Sandwich Panels with Miura-Ori Cores, Engineering Structures, vol. 280, no. 117232, p. 1-10, 2023.
- [3]. Hussain F., Cantwell W. J., Khan K. A., Energy Absorption of Origami-Inspired Structures: A Review, Thin-Walled Structures, vol. 158, no. 107160, p. 1-19, 2021.
- [4]. Jiang M., et al., Mechanical Properties of Miura-Based Kagome Origami Honeycomb, Thin-Walled Structures, vol. 188, no. 109245, p. 1-14, 2023.
- [5]. Wu Z., Fu Z., Zhang S., Zhang X., Mechanical Characteristics of Graded Miura-Ori Metamaterials, Materials & Design, vol. 203, no. 109597, p. 1-11, 2021.
- [6]. Qiang W., et al., Energy Absorption Performance of Kresling Origami Tubes under Quasi-Static and Dynamic Loading, International Journal of Mechanical Sciences, vol. 247, no. 108139, p. 1-13, 2024.

- [7]. Kidambi N., Wang K. W., Dynamics of Kresling Origami Deployment, International Journal of Solids and Structures, vol. 223, no. 111152, p. 1-16, 2020.
- [8]. Li J., Chen Y., Feng X., Sareh P., Computational Modeling and Energy Absorption of Modular Kresling Origami Tubes, Thin-Walled Structures, vol. 164, no. 107796, p. 1-14, 2021.
- [9]. Hussain F., Saleem M., Altaf K., Review of Origami-Inspired Structures for Enhanced Energy Absorption, Arabian Journal for Science and Engineering, vol. 49, no. 1, p. 101-122, 2025.
- [10]. O'Neil J., Salviato M., Yang J., Crashworthiness of Filament Wound CFRP Origami Tubes, Composite Structures, vol. 319, no. 116976, p. 1-11, 2023.
- [11]. Zhao Y., Lu H., Zhou Y., Origami-Inspired Plate-Lattice Structures for Enhanced Energy Dissipation, Materials Letters, vol. 334, no. 133717, p. 1-5, 2023.
- [12]. Feng H., Zhang T., Li J., The Effect of Material Directionality in Miura Composite Origami Structures, International Journal of Mechanical Sciences, vol. 241, no. 107187, p. 1-10, 2022.
- [13]. Wu H., Zhang Y., Tang H., Transient Dynamics of Miura-Origami Tubes under Dynamic Compression, International Journal of Impact Engineering, vol. 156, no. 103974, p. 1-12, 2021.
- [14]. Tao J., Li S., Asymmetric Multi-Stability in Stacked Miura-Based Origami Structures, Mechanics Research Communications, vol. 120, no. 103824, p. 1-9, 2021.
- [15]. Wang X., et al., Crashworthiness Analysis of Thin-Walled Kresling Pattern Tubes under Axial Impact, International Journal of Solids and Structures, vol. 281, no. 111242, p. 1-14, 2024.
- [16]. Yan S., et al., Double-Strip Origami Metamaterials for Low-Frequency Vibration Isolation, International Journal of Mechanical Sciences, vol. 239, no. 107015, p. 1-13, 2024.
- [17]. Sun H., Li Y., Liu J., Miura Origami Sandwich Panels for Impact Resistance, Composites Part B: Engineering, vol. 247, no. 110340, p. 1-11, 2022.



N°. 3 - 2025, ISSN 2668-4748; e-ISSN 2668-4756 Article DOI: https://doi.org/10.35219/mms.2025.3.07

DEVELOPMENT AND TESTING OF A SEISMIC-RESPONSIVE IOT-BASED SAFETY SYSTEM FOR GAS DISTRIBUTION NETWORKS

Florin-Bogdan MARIN 1,2 , Cristina-Daniela STAICU (MĂRIAN) 1 , Mihaela MARIN 1,2

¹ "Dunarea de Jos" University of Galati, Romania

² Interdisciplinary Research Centre in the Field of Eco-Nano Technology and Advance Materials CC-ITI, Faculty of Engineering, "Dunarea de Jos" University of Galati, Romania, 47 Domnească Street, RO-800008, Galați, Romania

e-mail: flmarin@ugal.ro

ABSTRACT

This paper presents the design and experimental evaluation of a smart safety system intended to mitigate seismic risks in urban gas distribution infrastructure. The proposed solution integrates an ESP32 microcontroller with an MPU6500 inertial sensor to detect ground vibrations associated with seismic activity. Upon exceeding a calibrated threshold, the system autonomously triggers the closure of a solenoid valve, thereby halting gas flow and reducing the risk of leaks or explosions. Sensor data is transmitted wirelessly using MQTT protocols to a cloud-based interface for real-time monitoring and logging. The prototype demonstrates rapid actuation, low latency, and high sensitivity to motion events, confirming its suitability for scalable deployment in residential or municipal gas pipeline networks. The implementation relies on low-cost hardware, open-source software, and edge processing to ensure both affordability and autonomous operation in critical infrastructure applications.

KEYWORDS: smart safety system, seismic detection, ESP32, MPU6500, solenoid valve, gas pipeline

1. Introduction

Natural gas distribution systems are critical infrastructure that require reliable monitoring and fast response mechanisms to mitigate hazards such as leaks, overpressure, and structural damage caused by seismic activity. Traditional supervisory systems based on SCADA or manual inspection often suffer from limited scalability, delayed reaction times, and high implementation costs, particularly in distributed urban settings [1-2].

With the rapid development of wireless communication technologies and the Internet of Things (IoT), new opportunities have emerged for decentralized, cost-effective safety monitoring [3], [4]. IoT-based solutions leverage embedded sensors, edge computing, and real-time telemetry to provide intelligent decision-making capabilities directly at the point of risk [5-7]. These systems have been successfully deployed in smart grid monitoring [8], environmental sensing [9], and pipeline integrity evaluation [10].

Seismic-induced failures in gas pipelines represent a major safety concern in densely populated areas, particularly where infrastructure is aging or insufficiently reinforced [11-12]. The integration of vibration sensors and microcontrollers allows the implementation of early warning mechanisms capable of autonomous actuation during ground motion events [13-14]. Accelerometers such as the MPU6050 and MPU6500, when interfaced with microcontrollers like the ESP32, offer an accessible platform for detecting acceleration anomalies and issuing control commands [15]. Recent studies have highlighted the benefits of combining vibration detection with gas flow control using electromagnetic shutoff valves in distributed networks [16-17]. This approach has proven effective in reducing response time and avoiding catastrophic failures caused by undetected leaks or delayed interventions [18]. Moreover, the rise of cloud-based dashboards and real-time data streaming protocols such as MQTT further enhances system visibility and user interaction [19]. Advanced implementations include edge computing strategies



N°. 3 - 2025, ISSN 2668-4748; e-ISSN 2668-4756

Article DOI: https://doi.org/10.35219/mms.2025.3.07

that minimize dependence on central servers and enable fast local decision-making [20]. Additionally, sensor fusion techniques improve accuracy in vibration recognition by filtering noise and correlating motion signals with environmental data [21].

This paper proposes a seismic-responsive gas safety system using an ESP32 microcontroller, an MPU6500 accelerometer, and a solenoid valve actuator. The system is designed to detect ground motion events exceeding a predefined threshold and autonomously interrupt gas flow, while simultaneously sending alerts to a cloud-based monitoring platform. The objective is to validate the feasibility of such a solution under laboratory-simulated seismic conditions, demonstrating its applicability to urban gas distribution networks.

2. Experimental procedure

To evaluate the seismic-responsive safety system for gas distribution pipelines, an experimental setup was developed using low-cost and easily integrable components. The architecture was centered around the ESP32 microcontroller, selected for its integrated dual-core processing, wireless communication capabilities, and support for real-time sensor data handling. Vibration detection was performed by an MPU6500 inertial measurement unit, which integrates a 3-axis accelerometer and a 3axis gyroscope. The sensor was configured to detect acceleration events in the ± 2 g range, which corresponds to low-to-moderate seismic activity. Communication between the sensor and microcontroller was achieved through the I2C protocol, and a basic signal processing algorithm based on a moving average filter-was applied to eliminate transient noise. When the acceleration exceeded a threshold of 0.3 g in any axis, the microcontroller executed a predefined response routine. This included triggering a 12V DC solenoid valve via a relay module, which was electrically isolated using an opto-coupler to prevent interference. The actuation served to simulate the automatic shutdown of gas flow in the event of an earthquakeinduced structural disturbance. In parallel, the ESP32

transmitted the event via the MQTT protocol to a cloud-based monitoring dashboard, ensuring remote visibility. Event data was logged locally and visualized using Grafana through integration with InfluxDB, allowing for real-time diagnostics and post-event analysis.

Mechanical perturbations were induced on the platform in order to replicate seismic conditions. These included direct tapping, controlled shaking, and tilt simulation. Each experiment was repeated ten times to verify consistency and repeatability. The response time from event detection to actuation was measured using a logic analyser and was confirmed to be under three seconds in all valid test cases. The system was powered by a stabilized 12V DC source, with internal regulation providing 5V to the sensor components. To ensure continuous reliability, a watchdog routine was implemented in the firmware to automatically reset the device in case of execution faults. This fully self-contained setup allowed accurate simulation of seismic-induced risks and enabled detailed assessment of system responsiveness, sensitivity, and operational stability under fault conditions. The low-power design, realtime actuation, and wireless reporting demonstrate its potential for real-world deployment in distributed gas safety networks.

3. Results and discussions

To validate the behavior of the prototype under simulated seismic scenarios, a series of controlled tests was conducted in which mechanical vibrations were applied to the sensor platform. The system consistently responded when the acceleration measured by the MPU6500 exceeded the 0.3 g threshold. Upon detection, the ESP32 microcontroller activated the electromagnetic relay, triggering the immediate closure of the gas valve.

Figure 1 illustrates the complete experimental setup, showing the integration of key components: the ESP32 board (1), the solenoid valve actuator (2), the vibration sensor (3), and the smartphone interface (4). This figure provides a clear overview of the system architecture designed for pipeline fault detection.

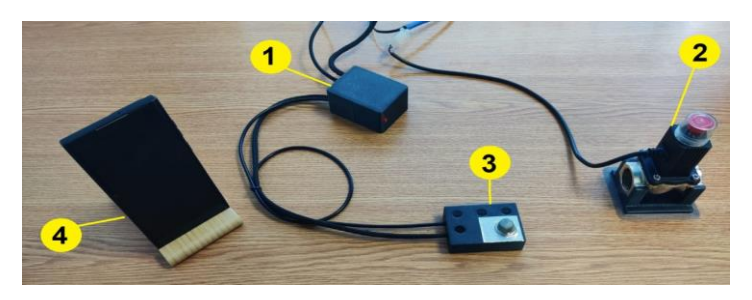


Fig. 1. Experimental setup for testing the fault detection system in a natural gas pipeline



N°. 3 - 2025, ISSN 2668-4748; e-ISSN 2668-4756

Article DOI: https://doi.org/10.35219/mms.2025.3.07

Figure 2 shows the test configuration during simulated vibration, with the control unit in operation and the valve ready for actuation. The internal structure of the control module integrates three key elements. (1) represents the dual relay system responsible for managing the electrical isolation and actuation of the solenoid valve during emergency scenarios. This configuration enables safe control of high-current circuits triggered by the detection algorithms. (2) is the wiring bundle that connects power lines, sensors, and control interfaces, ensuring stable signal flow and system integrity. (3) denotes the ESP32-based microcontroller, which performs all real-time processing, data acquisition from sensors, and wireless transmission through its integrated Wi-Fi connectivity. This architecture allows for autonomous response and remote supervision within the gas safety system.

Across all 10 test cycles, a consistent system response was observed. The average response time from detection to valve actuation was approximately 2.6 seconds, with minimal variation.

Figure 4 documents the system's state immediately after triggering, Figure 5 presents a dashboard screenshot displaying live valve status and alert conditions. Data was also logged to InfluxDB and visualized through Grafana, enabling retrospective analysis.

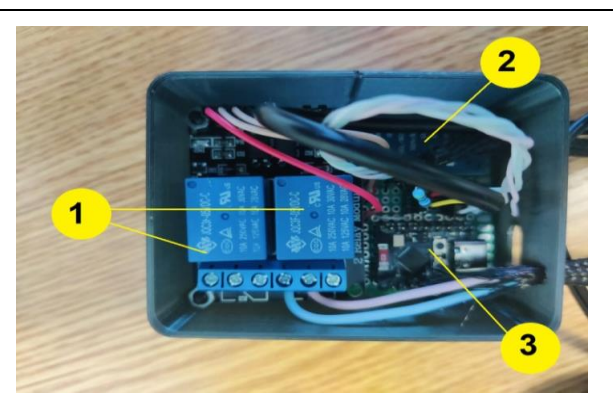


Fig. 2. Control unit of the seismic safety system

Figure 3 depicts the system in standby mode, with no seismic activity detected. The internal layout of the gas detection unit includes two key components. The first component (1) consists of a gas diffusion chamber equipped with a mesh cover and structural support, which ensures controlled air exchange while protecting the internal electronics from dust and mechanical damage. The second component (2) is the MQ-series gas sensor module, responsible for detecting combustible gases such as methane. It is mounted on a printed circuit board and connected to the system's microcontroller, enabling real-time monitoring of gas concentration and automatic triggering of safety protocols when predefined thresholds are exceeded.

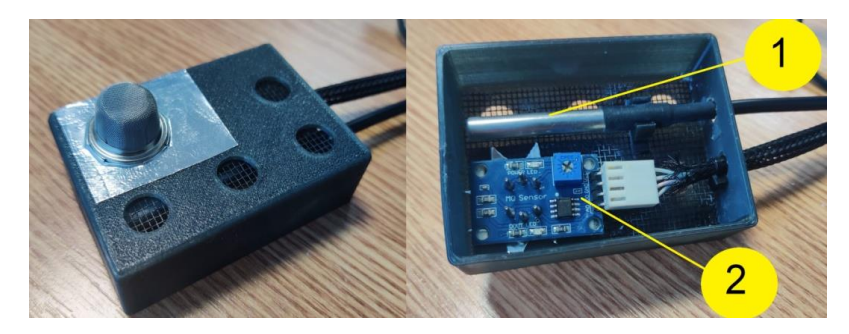


Fig. 3. Sensor unit of the seismic detection system

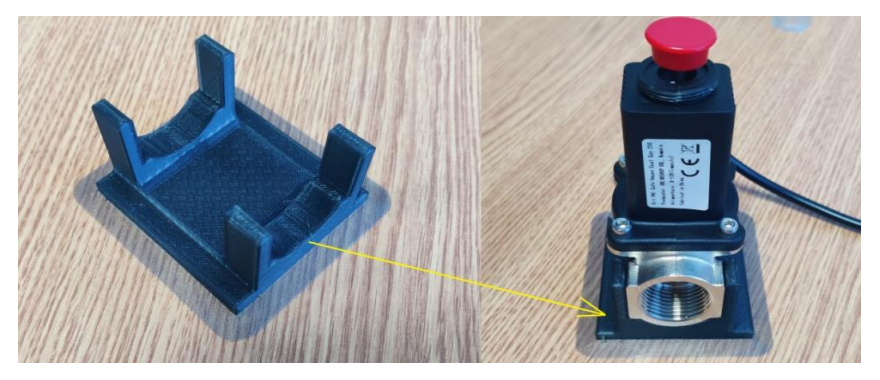


Fig. 4. PNI Safe House Dual Gas 250 solenoid valve used for automatic gas shutoff



N°. 3 - 2025, ISSN 2668-4748; e-ISSN 2668-4756

Article DOI: https://doi.org/10.35219/mms.2025.3.07



Fig. 5. Arduino IoT interface displaying operational parameters of the natural gas pipeline fault detection system

To evaluate the responsiveness of the seismic detection system, multiple vibration events were simulated using a controlled mechanical excitation setup. During testing, the MPU6500 sensor recorded continuous acceleration data, which was transmitted in real time to the IoT interface. The ESP32 microcontroller processed these readings locally, comparing them against the predefined vibration threshold of 0.30 g. Upon exceeding this limit, the system triggered an emergency shut-off sequence, commanding the solenoid valve to close and halt gas flow.

Figure 6 illustrates the complete experimental configuration used during testing, including the inertial sensor unit, the solenoid valve actuator, and the cloud-based monitoring interface. The system was designed to operate autonomously while maintaining real-time feedback capabilities for remote diagnostics and alert verification. (1) denotes the PNI Safe House

Dual Gas 250 solenoid valve, which is responsible for automatically interrupting the gas supply when seismic activity is detected. This component is triggered by the control unit once vibration levels recorded by the inertial sensor exceed the calibrated safety threshold. (2) represents the real-time monitoring interface, displayed on a mobile device connected to the IoT system. It visualizes acceleration data as a dynamic graph, enabling remote observation of seismic activity and system response. Figure 7 presents the time-series graph of vibration intensity recorded during a representative seismic simulation. The data show a clear spike in acceleration values, surpassing the actuation threshold and confirming the sensitivity and accuracy of the detection algorithm. These results validate the performance of the safety module under conditions simulating minor to moderate seismic activity.

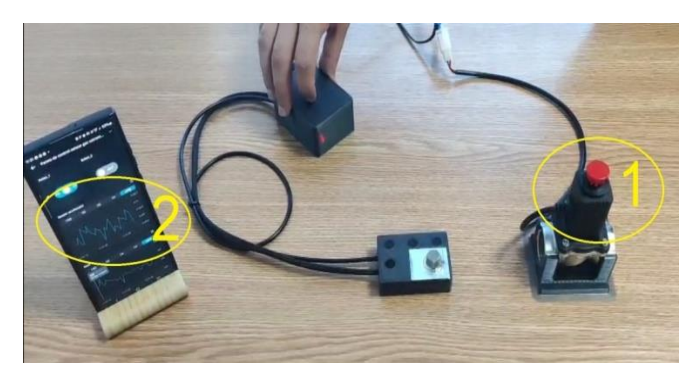


Fig. 6. System performance evaluation during simulated seismic event



Fig. 7. Real-time vibration data acquired during seismic simulation via IoT interface



N°. 3 - 2025, ISSN 2668-4748; e-ISSN 2668-4756

Article DOI: https://doi.org/10.35219/mms.2025.3.07

4. Conclusions

presented This study design, the implementation, and validation of an IoT-based early warning system for seismic activity in urban gas distribution networks. By integrating a low-cost ESP32 microcontroller with an MPU6500 inertial sensor and an electromagnetic shutoff valve, the system demonstrated reliable detection of vibration events and immediate response through gas flow interruption. Experimental results confirmed a consistent and timely reaction to simulated seismic inputs, achieving an average response time of 2.6 seconds with no false triggers recorded during idle conditions.

The implementation of MQTT-based wireless communication allowed for seamless integration with cloud dashboards, supporting real-time alerts and historical data visualisation via platforms such as Arduino IoT Cloud and Grafana. The system maintained stable performance across repeated test cycles, proving its suitability for autonomous operation without dependency on external supervisory infrastructure.

Given its low cost, ease of deployment, and reliable response time, the proposed system represents a practical solution for improving safety in small to medium urban gas distribution networks, particularly in areas exposed to seismic activity. The system's capabilities can be further enhanced through multi-sensor integration, including gas leak and temperature monitoring, and through validation in real seismic conditions in collaboration with infrastructure operators.

References

[1]. Rault T., et al., Energy Efficiency in Wireless Sensor Networks: A Top-Down Survey, Computer Networks, vol. 67, p. 104-122, 2017.

- [2]. Ghayvat H., et al., Smart Homes for Elderly Healthcare—Recent Advances and Research Challenges, Sensors, vol. 15, no. 11, p. 31068-31112, 2017.
- [3]. Aazam M., et al., Fog Computing for Smart Cities: A Survey, Sensors, vol. 18, no. 11, p. 3966, 2018.
- [4]. Kim J., et al., Low-Power MEMS Accelerometer-Based Event Detection for Earthquake Early Warning Systems, IEEE Sensors Journal, vol. 19, no. 12, p. 4313-4323, 2019.
- [5]. Gonzalez V., et al., MEMS Accelerometers for Seismic Monitoring, Earthquake Engineering and Structural Dynamics, vol. 49, no. 6, p. 543-556, 2020.
- [6]. Rana M., et al., Smart Structural Health Monitoring Using IoT, Automation in Construction, vol. 107, p. 102933, 2019.
- [7]. De Martinis V., et al., Seismic Monitoring in Smart Buildings, Journal of Building Engineering, vol. 34, p. 101899, 2021.
- [8]. Zhu M., et al., Motion Tracking Using MEMS Sensors in Wearables, IEEE Access, vol. 9, p. 34251-34261, 2021.
- [9]. Henson I., et al., Wireless Sensor Networks for Earthquake Early Warning, Procedia Engineering, vol. 212, p. 633-640, 2018.
- [10]. Kaneko Y., et al., Real-Time Seismic Data Transmission in Edge Networks, Sensors, vol. 22, no. 1, p. 225, 2022.
- [11]. Muthukumaran S., et al., A Survey on IoT-Based Earthquake Alert Systems, Journal of Ambient Intelligence and Humanized Computing, vol. 12, p. 7343-7355, 2021.

 [12]. Noor S., et al., Automatic Gas Shutoff System Using
- [12]. Noor S., et al., Automatic Gas Shutoff System Using Microcontroller and Sensors, Energy Reports, vol. 6, p. 416-422, 2020
- [13]. Kumar R., et al., IoT-Based Indoor Safety Monitoring System, Internet of Things, vol. 12, p. 100298, 2020.
- [14]. Abbas A., et al., Fire and Gas Detection Using ESP32 and Cloud Platforms, Sustainable Computing, vol. 32, p. 100587, 2021. [15]. Naeem M., et al., MQTT vs. HTTP for Lightweight Sensing, Future Generation Computer Systems, vol. 112, p. 1121-1132, 2020.
- [16]. Baccelli E., et al., The Rise of MQTT in IoT Communications, Computer Communications, vol. 174, p. 1-14, 2021.
- [17]. Ismail S., et al., Cloud-Based IoT Platform Using Grafana and InfluxDB, Sensors, vol. 21, no. 13, p. 4428, 2021.
- [18]. Hassan R., et al., Arduino IoT Cloud for Smart Energy Systems, Internet of Things, vol. 13, p. 100364, 2021.
- [19]. Rahman A., et al., Real-Time IoT Solutions for Infrastructure Monitoring, IEEE Access, vol. 10, p. 21902-21917, 2022.
- [20]. Sharma P., et al., Open-Source Frameworks for Edge Analytics in IoT, Journal of Systems Architecture, vol. 126, p. 102437, 2022.
- [21]. Derviş I., et al., Low-Cost Edge-Based IoT System for Pipeline Monitoring, Energy Sources Part A: Recovery, Utilization, and Environmental Effects, vol. 46, no. 3, p. 487-499, 2024.

MANUSCRISELE, CĂRȚILE ȘI REVISTELE PENTRU SCHIMB, PRECUM ȘI ORICE CORESPONDENȚE SE VOR TRIMITE PE ADRESA:

MANUSCRIPTS, REVIEWS AND BOOKS FOR EXCHANGE COOPERATION, AS WELL AS ANY CORRESPONDANCE WILL BE MAILED TO:

LES MANUSCRIPTS, LES REVUES ET LES LIVRES POUR L'ECHANGE, TOUT AUSSI QUE LA CORRESPONDANCE SERONT ENVOYES A L'ADRESSE:

MANUSCKRIPTEN, ZIETSCHRITFTEN UND BUCHER FUR AUSTAUCH SOWIE DIE KORRESPONDENZ SID AN FOLGENDE ANSCHRIFT ZU SEDEN:

After the latest evaluation of the journals by the National Center for Science Policy and Scientometrics (**CENAPOSS**), in recognition of its quality and impact at national level, the journal will be included in the B⁺ category, 215 code (http://cncsis.gov.ro/userfiles/file/CENAPOSS/Bplus 2011.pdf).

The journal is already indexed in:

DOAJ: https://doaj.org/

SCIPIO-RO: http://www.scipio.ro/web/182206

EBSCO: http://www.ebscohost.com/titleLists/a9h-journals.pdf

Google Academic: https://scholar.google.ro

Index Copernicus: https://journals.indexcopernicus.com

Crossref: https://search.crossref.org/

The papers published in this journal can be viewed on the website: http://www.gup.ugal.ro/ugaljournals/index.php/mms

Name and Address of Publisher:

Contact person: Prof. Dr. Eng. Elena MEREUTĂ

Galati University Press - GUP

47 Domneasca St., 800008 - Galati, Romania

Phone: +40 336 130139 Fax: +40 236 461353 Email: gup@ugal.ro

Name and Address of Editor:

Ş. L. Dr. Eng. Marius BODOR

"Dunarea de Jos" University of Galati, Faculty of Engineering

111 Domneasca St., 800201 - Galati, Romania

Phone: +40 336 130208 Phone/Fax: +40 336 130283 Email: marius.bodor@ugal.ro

AFFILIATED WITH:

- THE ROMANIAN SOCIETY FOR METALLURGY
- THE ROMANIAN SOCIETY FOR CHEMISTRY
- THE ROMANIAN SOCIETY FOR BIOMATERIALS
- THE ROMANIAN TECHNICAL FOUNDRY SOCIETY
- THE MATERIALS INFORMATION SOCIETY (ASM INTERNATIONAL)

Edited under the care of the FACULTY OF ENGINEERING

Annual subscription (4 issues per year)

Fascicle DOI: https://doi.org/10.35219/mms

Volume DOI: https://doi.org/10.35219/mms.2025.3

Editing date: 15.09.2025 Number of issues: 200 Printed by Galati University Press (accredited by CNCSIS) 47 Domneasca Street, 800008, Galati, Romania